AD NUMBER
AD093842
CLASSIFICATION CHANGES
TO: unclassified
FROM: confidential
LIMITATION CHANGES
TO: Approved for public release, distribution unlimited
FROM: Distribution authorized to U.S. Gov't. agencies and their contractors; Administrative/Operational Use; 26 MAR 1956. Other requests shall be referred to National Aeronautics and Space Administration, Washington, DC.
AUTHORITY
NASA TR SERVER WEBSITE; NASA TR SERVER WEBSITE

NOTICE: THIS DOCUMENT CONTAINS INFORMATION AFFECTING THE NATIONAL DEFENSE OF THE UNITED STATES WITHIN THE MEANING OF THE ESPIONAGE LAWS, TITLE 18, U.S.C., SECTIONS 793 and 794. THE TRANSMISSION OR THE REVELATION OF ITS CONTENTS IN ANY MANNER TO AN UNAUTHORIZED PERSON IS PROHIBITED BY LAW.

Copy 25
RM A55L08

RESEARCH MEMORANDUM

A THEORETICAL STUDY OF THE LIFTING EFFICIENCY AT SUPERSONIC SPEEDS OF WINGS UTILIZING INDIRECT LIFT INDUCED BY VERTICAL SURFACES

By Vernon J. Rossow

Ames Aeronautical Laboratory
Moffett Field, Calif.

FC

CLASSIFIED DOCUMENT

This material contains information affecting the National Defense of the United States within the meaning of the espionage laws, Title 18, U.S.C., Secs. 793 and 794, the transmission or revelation of which in any manner to an unauthorized person is prohibited by law.

NATIONAL ADVISORY COMMITTEE
FOR AERONAUTICS

WASHINGTON

March 26, 1956

TABLE OF CONTENTS

TABLE OF CONTENTS - Concluded

NATIONAL ADVISORY COMMITTEE FOR AERONAUTICS

RESEARCH MEMORANDUM

A THEORETICAL STUDY OF THE LIFTING EFFICIENCY AT SUPERSONIC SPEEDS OF WINGS UTILIZING INDIRECT LIFT INDUCED BY VERTICAL SURFACES

By Vernon J. Rossow

SUMMARY

A theoretical study is made of the possibility of improving the lifting efficiency of aircraft flying at supersonic speeds by using the indirect lift which can be induced on the wing by the fuselage shape and/or wing end plates. This investigation is carried out by analyzing a number of special models which have surfaces so located and inclined to the free stream that pressure shadows are cast over the wing surface. The major portion of this study is carried out using linearized or first-order theory. The method of calculating the pressures on each model is described and graphs of the final results are presented.

The results indicate that in certain cases the lifting efficiency of a planar wing may be improved by favorable interference induced by lateral forces on the end plates or on the sides of the fuselage. At low values of reduced aspect ratio several of the airfoil systems studied are more efficient than is theoretically possible with planar wings. A configuration of comparable efficiency with a very high narrow fuselage is found for the higher values of reduced aspect ratio. In addition to improving the lifting efficiency of the aircraft, these indirect lift devices may also be used as control or stabilizing surfaces.

INTRODUCTION

Bodies or wings traveling at supersonic speeds cause disturbances that may extend for great distances without marked attenuation. Furthermore, a body traveling in the wave disturbance originated by another body may receive indirectly an aerodynamic force greater than that appearing on the body which originates the disturbance. This property of supersonic disturbances leads to consideration of the possibility of generating lift on a wing indirectly, or by interference. Effects of this type may possibly be used to increase the efficiency of the airplane by reducing the drag due to thickness or to lift. Either or both may be accomplished by favorable interference between the fuselage and the wing and in some cases between wing end plates and the wing.

The two-dimensional supersonic wind-tunnel nozzle is a classic example in which forces are induced indirectly. The pressure waves generated by the nozzle contour are cast across the flat wind-tunnel side walls which are alined with the stream direction. Since the side walls do not induce pressures, the side forces arise entirely from the indirect force induced by the nozzle contour. If a particular portion of this flow field is selected and placed in a supersonic stream, it could represent a wing (side-wall section) at zero angle of attack with lift induced on it by end plates (sections of the nozzle) which are deflected. It was the consideration of this analogy which led the author to the investigation reported herein.

The use of end plates on wings at subsonic and supersonic speeds has been studied by numerous authors. For example, see references 1 through 4, Reid, Hemke, Scholkemeir, and Gorgui, respectively. In general, these investigations considered the end plates as being fixed. Several of the studies included configurations wherein a portion of the end plate was movable. The movable parts were deflected in the same direction above and below the wing. The extension to "canted adjustable end plates" at subsonic speeds was investigated by Clements in reference 5.[1] The wing-end-plate combinations studied consisted of a straight wing with end plates. The parts of the end plates above and below the wing could be deflected independently to produce desired effects on the take-off and landing characteristics.

The possibility of utilizing vertical surfaces on the fuselage to produce indirect lift at supersonic speeds has been studied by Ferri, Clarke, and Cassaccio in reference 6. The special configurations which they considered consist of a body with several flat sections that receive pressures from, and induce pressures on, a wing. Two wing plan forms were considered, a delta wing and a particular tapered wing with the leading edges swept along the Mach lines. The trailing edge of the tapered wing was the hyperbolic intersection of the Mach cone from the body edge with the wing. The pressure fields were found by linearized theory and were integrated to obtain lift and drag.

This report extends the study of interfering pressure fields at supersonic speeds by considering models that have swept wings, end plates, and specially shaped bodies. All these factors are varied to try to find an efficient lifting system. In a study of this type, the shape of the various components of the airfoil systems may be varied throughout wide limits so that the possible number of designs is unlimited. However, by choosing several models which are relatively easy to analyze, it is at least possible to discover which characteristics of the various models are desirable and to make improvements accordingly.

[1] The use of wing end plates deflected differentially for lift augmentation and roll control was proposed in a patent application by John A. Axelson of Ames Aeronautical Laboratory.

SYMBOLS

A	aspect ratio of wing, $\frac{(\text{span})^2}{\text{area}}$
b	one-half wing span
c	chord length of wing
C_L	lift coefficient
C_{D_i}	coefficient of drag due to lift
C_p	pressure coefficient, $\frac{p - p_\infty}{q_\infty}$
D	drag
G	See equation (17).
h	height of rectangular part of fin (See sketch (j).)
i	$\sqrt{-1}$
L	lift
m	ratio of tangent of leading- or trailing-edge angle to tangent of Mach angle (β tan Λ)
M	Mach number
p	static pressure
q	dynamic pressure
Re	real part of expression
S	area of wing
T	thrust on the fuselage
u,v,w	velocity perturbations in x,y,z directions, respectively
U	free-stream velocity
x,y,z	rectangular coordinate system (The free stream is in the x direction.)
x_m	See equation (16).
$\bar{z}$	See equation (6c).

$\bar{z}$ See equation (15).

z_h See equation (23) and sketch (k).

α angle of attack

β $\sqrt{M^2 - 1}$

δ deflection angle of fin or half-angle of cone

σ optimum ratio of angle of attack of horizontal to vertical surface, $\frac{\alpha}{\delta}$

ϵ conical flow parameter, $\frac{y + iz}{x + \sqrt{x^2 - y^2 - z^2}}$

τ conical flow parameter, $\frac{2\epsilon}{1 + \epsilon^2}$

Λ sweep angle of leading or trailing edge

Subscripts

∞ free stream

A,B particular regions on wing

b body

c half-cone contribution

c-h cone interference on wing

h horizontal surface or wing

h-b quantities arising from interference of horizontal surface on body

h-c quantities arising from interference of horizontal surface on cone

h-h quantities arising from interference of horizontal surface on itself

h-v quantities arising from interference of horizontal surface on vertical surface

t leading-edge thrust

v-b quantities arising from interference of vertical surface on body

v-h quantities arising from interference of vertical surface on horizontal surface

v-v quantities arising from vertical surface interfering on itself

I,II, III,IV, V } conical-flow solutions (See sketches (b) and (d).)

Superscripts

( )' first derivative with respect to deflection angle

( )" second derivative with respect to deflection angle

SCOPE

The models that are studied may be divided into two general groups. The first group consists of combinations of flat vertical and horizontal surfaces of zero thickness without a fuselage. The second group includes a fuselage. A sketch of each of the models analyzed in this report is shown in figure 1.

The pressures acting on the various surfaces of the models are calculated from conical-flow solutions derived by linear theory or by a superposition of several such solutions. A discussion of conical flow or of the method of finding the various solutions used herein is not given because the subject is adequately covered in references 7 and 8. The conical-flow solutions are taken directly from table A, 13a of reference 8,[2] and applied to the problem at hand. The deflections of the various surfaces are assumed small enough so that linear theory and the linearized pressure relation,

$$C_p = \frac{-2u}{U} \tag{1}$$

will apply with reasonable accuracy. Equation (1) is used throughout the analysis unless otherwise stated. In this way the lift and the drag coefficients and the drag factor $C_{D_i}/\beta C_L^2$ of the various models are calculated for a range of reduced aspect ratios, βA. The coefficients are

[2]The availability of this table avoids the necessity of finding each solution by linear theory and shortens the analysis considerably.

computed using both the plan-form area and the plan-form plus fin area, as reference area, thereby permitting a comparison to be made with standard wings under conditions wherein the end plates or fins may or may not serve as necessary vertical-tail surfaces. When the vertical surface is considered as part of the fuselage, it is never included in the reference area.

In order to simplify the calculations and the equations, the results are calculated for $M = \sqrt{2}$. By use of the Prandtl-Glauert transformation, these results are extended to other Mach numbers, and shown in the various figures in a form that contains the Mach number as a parameter.

The drag factor $C_{D_i}/\beta C_L^2$ is used as the basis of comparison of the lifting efficiency of the various models. Its importance arises from its relation to the maximum lift-drag ratio expressed as

$$\left(\frac{L}{D}\right)_{max} = \frac{1}{2\sqrt{C_{D_o}(C_{D_i}/C_L^2)}} \tag{2}$$

The coefficient C_{D_o} expresses the drag of the whole airplane at zero lift, that is, when all the surfaces are undeflected. It includes the viscous and the thickness drag of the wing, fuselage, and auxiliary surfaces. Effects of flow separation or possible effects of boundary-layer thickening on the various surfaces or surface junctures are not considered. The coefficient of the pressure drag due to lift is C_{D_i} and the lift coefficient is C_L. It is assumed that C_L is proportional to the angle of attack and C_{D_i} to the square of the angle of attack, that is, a parabolic lift-drag polar. All of the models, except number 10, theoretically have parabolic lift-drag polars. The advantage of using the drag factor is that it is independent of angle of attack. It also affords a comparison of the lifting efficiency of the various airfoil combinations without fixing the thickness of the surfaces, the fuselage shape, or the viscous drag of the aircraft.

It is necessary to establish reference models whereby the new lifting systems can be judged as worthy or unworthy of further consideration. The reference models chosen for the drag factor are the triangular wing, the constant-chord swept wing, and the theoretical minimum for slender wings of zero thickness. The results for these reference planar wings are shown on the various graphs as the dashed lines. The parameters for the triangular wing are from reference 9, those for the constant-chord swept wing from reference 10, and those for the theoretical minimum from reference 11.

The reciprocity relations discussed in references 12 and 13 may be applied to all the models treated herein provided that in the reversed flow field the wing is warped to carry the same lift. The drag and lift of the reversed flow model are the same as the model in forward motion and therefore the lifting efficiency will also be the same. The results

of this paper could then be extended to an equal number of models with modified wings which are flying in the opposite direction. This extension will not be made.

The various fin-wing combinations and the method of calculating the pressures on each of them will now be described. The reader not interested in the analysis of each model may go directly to the discussion of the results and the figures at the end of the report. The results of the calculations are presented in figures 2 through 7. The drag factor which is used in the comparison is shown in figures 8 through 11 as a function of reduced aspect ratio.

ANALYSIS OF AIRFOIL COMBINATIONS WITHOUT FUSELAGES

In this section, several combinations of vertical and horizontal surfaces are described and analyzed. The general procedure followed in each case is:

1. Model is described.

2. Wing and fin flow fields are divided into the various conical flows which are superimposed to determine the pressure on each element of surface.

3. Expression for pressure in each conical flow field is found from the general formulas of reference 8.

4. Expressions are combined and integrated for lift and drag coefficients.

Model 1 - Triangular Fins With Unswept Leading Edges and Sonic Trailing Edges

Description.- The first airfoil combination to be studied consists of a wing swept along the Mach lines with end plates or fins as shown in sketch (a). The fins have unswept leading edges and the trailing edges are swept along the Mach line. The wing is parallel to the free stream and therefore does not generate a pressure field directly. The portion of the fin extending above the horizontal surface is deflected so that an expansion field or negative pressure region is produced on the top of the horizontal surface or wing. The portion of

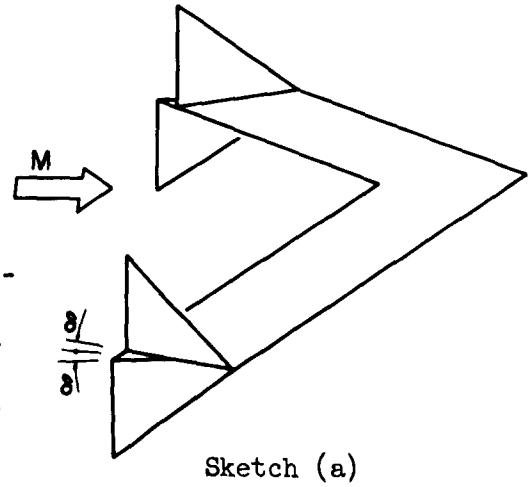

Sketch (a)

the fin extending below the wing is deflected so that a compression field or positive pressure region is produced on the bottom of the wing. The wing serves as a barrier between these opposite pressure fields. The deflections of both the upper and the lower parts of each end plate are always taken as equal and are considered positive when the lift generated by each is positive.

Lift.- On the wing of this first model, the pressure distribution is of the two-dimensional or Ackeret type ahead of the Mach cone from the fin tip. Inside this Mach cone the pressures take on a more complex form.

As pointed out previously, all edges of this configuration are either sonic or supersonic and therefore the flow field between the fins on top of the wing may be treated independently of the flow between the bottom fins. Also, since the upper and lower fins are deflected the same amount, the lift contribution induced by each may be considered equal within the linear approximation used in this analysis. The indirect lifting pressures within the Mach cone from the fin tip for the top side of the wing are calculated by superposition of several basic conical-flow solutions as illustrated in sketch (b). The values of u and w shown in the various regions

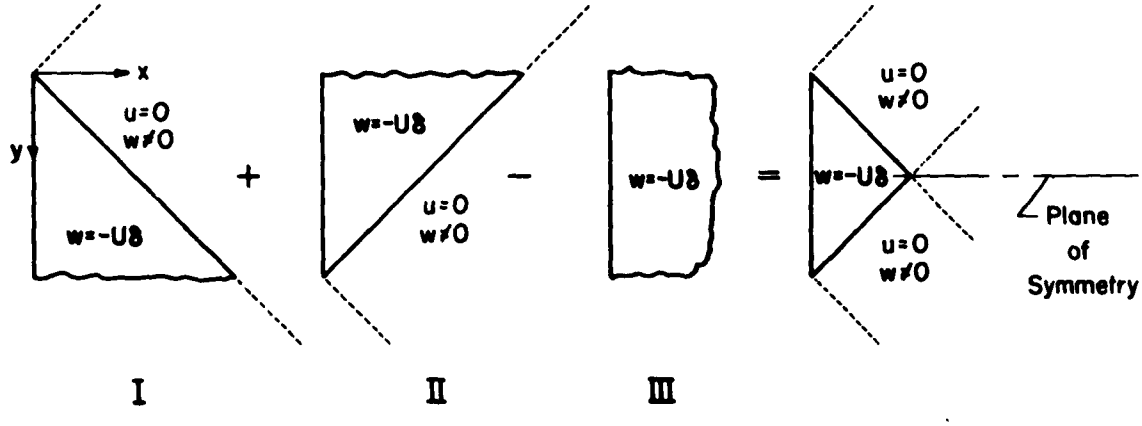

Sketch (b)

are the boundary conditions in the plane of the surface, z = 0. Addition of these flow solutions yields the solution together with the appropriate boundary conditions for the upper half of the fin and its image.

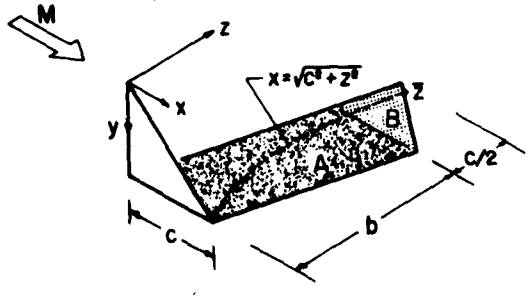

Sketch (c)

The resulting fin shape shown on the right of the sketch has a plane of symmetry which may be taken as a boundary. The wing is assumed to lie in this plane and serves as a reflecting plane. One half of the resultant flow field shown in sketch (b) is equivalent to the flow field between the fin and wing on the top (or bottom side, depending on which part of the flow field was chosen) as shown in sketch (c). The velocities in the flow

field inside the Mach cone from the fin tip which are induced by the conical surfaces shown in sketch (b) are found from table A, 13a of reference 8. The axial velocity for the first two parts are given by number 9 of this table as

$$u_I = \mathrm{Re}\,\frac{2m_2U\delta}{\pi\sqrt{m_2^2 - 1}}\tan^{-1}\sqrt{\frac{(m_2 - 1)(\tau - m_1)}{(m_2 - m_1)(1 - \tau)}}\Bigg|_{\substack{m_1 \to 1.0 \\ m_2 \to \infty}} \tag{3}$$

where m_1 and m_2 are the relative sweep angles of the trailing and leading edges, respectively, and

$$m = \beta \tan \Lambda \tag{4a}$$

$$\tau = \frac{2\epsilon}{1 + \epsilon^2} \tag{4b}$$

$$\epsilon = \frac{y + iz}{x + \sqrt{x^2 - y^2 - z^2}} \tag{4c}$$

After substitution of equations (4b) and (4c) into equation (3) and finding the real part at the above limits, the perturbation velocity in the x direction is,

$$u_I = \frac{U\delta}{\pi}\left(\tan^{-1}\frac{zy}{x^2 - z^2 + x\sqrt{x^2 - y^2 - z^2}} + 2\tan^{-1}\frac{z}{x - y + \sqrt{x^2 - y^2 - z^2}}\right) \tag{5a}$$

This expression is valid within the Mach cone from the fin tip; that is, $x^2 \geq y^2 + z^2$. Ahead of the Mach cone, $x^2 < y^2 + z^2$, the square root becomes imaginary and equation (5a) is not valid. However, the velocity ahead of the Mach cone is known to be the same as for two-dimensional flow,

$$u_I = U\delta \quad \text{for} \quad z \leq x \leq \sqrt{y^2 + z^2} \tag{5b}$$

On the surface of the wing, y = c, inside of the Mach cone from the fin tip the pressure coefficient is

$$C_p = -\frac{2u}{U} = -2\left(\frac{u_I}{U} + \frac{u_{II}}{U} - \frac{u_{III}}{U}\right)_{y=c} = -2\left(\frac{2u_I}{U} - \delta\right)_{y=c} \tag{5c}$$

since u_{II} is the same as u_I in the $y = c$ plane (i.e., the reflection plane or the plane of the wing) and $u_{III}/U = \delta$.

The pressures on the wing both inside of and forward of the Mach cone from the fin tip are now defined. The lift on the wing in these regions may be divided into two parts, A and B, as shown in sketch (c). Part A is the lift induced on the wing surface between $z = 0$ and $z = b$ and part B is the lift on the wing between $z = b$ and $b + (c/2)$. Region B is noted to be beyond the center of the whole configuration. On this part, lift is induced by fins at both wing tips, resulting in a doubling-up effect over the center sections. These parts may be written separately as,

$$C_{L_A} = \left(\int_0^b \int_{\sqrt{c^2+z^2}}^{c+z} C_p \, dx \, dz + \int_0^b \int_z^{\sqrt{c^2+z^2}} 4\delta \, dx \, dz \right) \frac{2}{S}$$

$$C_{L_B} = \left(\int_b^{\bar{z}} \int_{\sqrt{c^2+z^2}}^{2b+c-z} C_p \, dx \, dz - \int_b^{\bar{z}} \int_{\sqrt{c^2+z^2}}^{2b+c-z} 4\delta \, dx \, dz + \frac{4\delta c^2}{4} \right) \frac{2}{S}$$

which become

$$C_{L_A} = \frac{1}{bc + c^2} \left[\frac{8\delta}{\pi} \int_0^b \int_{\sqrt{c^2+z^2}}^{c+z} \left(\tan^{-1} \frac{zc}{x^2 - z^2 + x\sqrt{x^2 - c^2 - z^2}} + 2 \tan^{-1} \frac{z}{x - c + \sqrt{x^2 - c^2 - z^2}} \right) dx \, dz - 4\delta \int_0^b \left(z + c - \sqrt{c^2 + z^2} \right) dz + 4\delta \int_0^b \left(\sqrt{c^2 + z^2} - z \right) dz \right] \tag{6a}$$

$$C_{L_B} = \frac{1}{bc + c^2} \left[\frac{8\delta}{\pi} \int_b^{\bar{z}} \int_{\sqrt{c^2+z^2}}^{2b+c-z} \left(\tan^{-1} \frac{zc}{x^2 - z^2 + x\sqrt{x^2 - c^2 - z^2}} + 2 \tan^{-1} \frac{z}{x - c + \sqrt{x^2 - c^2 - z^2}} \right) dx \, dz - 8\delta \int_b^{\bar{z}} \left(2b + c - z - \sqrt{c^2 + z^2} \right) dz + 4\delta \frac{c^2}{4} \right] \tag{6b}$$

where

$$\bar{z} = \frac{(2b + c)^2 - c^2}{2(2b + c)} \tag{6c}$$

The total lift coefficient for the entire wing is the sum of equations (6a) and (6b), where the coefficient is based on plan area plus fin area, $2bc + 2c^2$. The integration with respect to x can be carried out easily. So, equations (6a) and (6b) become

$$C_{L_A} = \frac{8\delta}{\pi(bc + c^2)} \int_0^b \left\{ z \tan^{-1}\sqrt{\frac{2z}{c}} - \pi z + (z + c)\left[\tan^{-1} \frac{zc}{c^2 + 2cz + (c + z)\sqrt{2cz}} + 2 \tan^{-1} \frac{z}{z + \sqrt{2cz}} \right] + \right.$$

$$\left. z \ln \frac{c + z + \sqrt{2cz}}{\sqrt{c^2 + z^2}} + c \sin^{-1} \frac{c - z}{\sqrt{c^2 + z^2}} \right\} dz \qquad (7a)$$

$$C_{L_B} = \frac{\delta}{bc + c^2} \left(1 + \frac{8}{\pi} \int_b^{\bar{z}} \left\{ (2b + c - z)\left[\tan^{-1} \frac{zc}{(2b + c - z)^2 - z^2 + (2b + c - z)\sqrt{(2b + c - z)^2 - c^2 - z^2}} + \right.\right.\right.$$

$$\left. 2 \tan^{-1} \frac{z}{(2b - z) + \sqrt{(2b + c - z)^2 - c^2 - z^2}} \right] - \pi\sqrt{c^2 + z^2} + z \tan^{-1} \frac{\sqrt{(2b + c - z)^2 - c^2 - z^2}}{c} +$$

$$z \ln \frac{2b + c - z + \sqrt{(2b + c - z)^2 - c^2 - z^2}}{\sqrt{c^2 + z^2}} + c \sin^{-1} \frac{c(c + 2b - z - c) - z^2}{\sqrt{c^2 + z^2}\,(2b + c - z - c)} + \frac{\pi c}{2} -$$

$$\left.\left. \pi(2b + c - z - \sqrt{c^2 + z^2}) \right\} dz \right) \qquad (7b)$$

The integration over z is carried out graphically.

Since the wing has a constant chord, the aspect ratio is,

$$A = \frac{2b}{c} \qquad (8)$$

As pointed out above, these results are for $M = \sqrt{2}$. However, by application of the Prandtl-Glauert transformation the results of equations (7) and (8) can be extended to other Mach numbers. This transformation, of course, changes the proportions of all the airfoils to fit the changed

CONFIDENTIAL

geometry of the Mach waves. All the results of this paper will be extended in this manner without further reference to the Prandtl-Glauert rule.

Drag.- The horizontal surface on which the lift is acting is at zero angle of attack and of zero thickness. Therefore, it does not contribute to the pressure drag. The only drag arising is that of the deflected fins. It is to be noted that the inner side of all the fins is not influenced by any of the other surfaces. The pressure distribution on these surfaces is therefore the two-dimensional type, $C_p = \pm 2\delta$.

On the outer sides of the fins, velocities are induced by both the upper and the lower fins over a portion of the fin surfaces. Since they are deflected differentially, the drag is considerably less in this region of mutual influence. The drag of the outside of the fins is computed by superposition of the several conical flows as shown in sketch (d). The

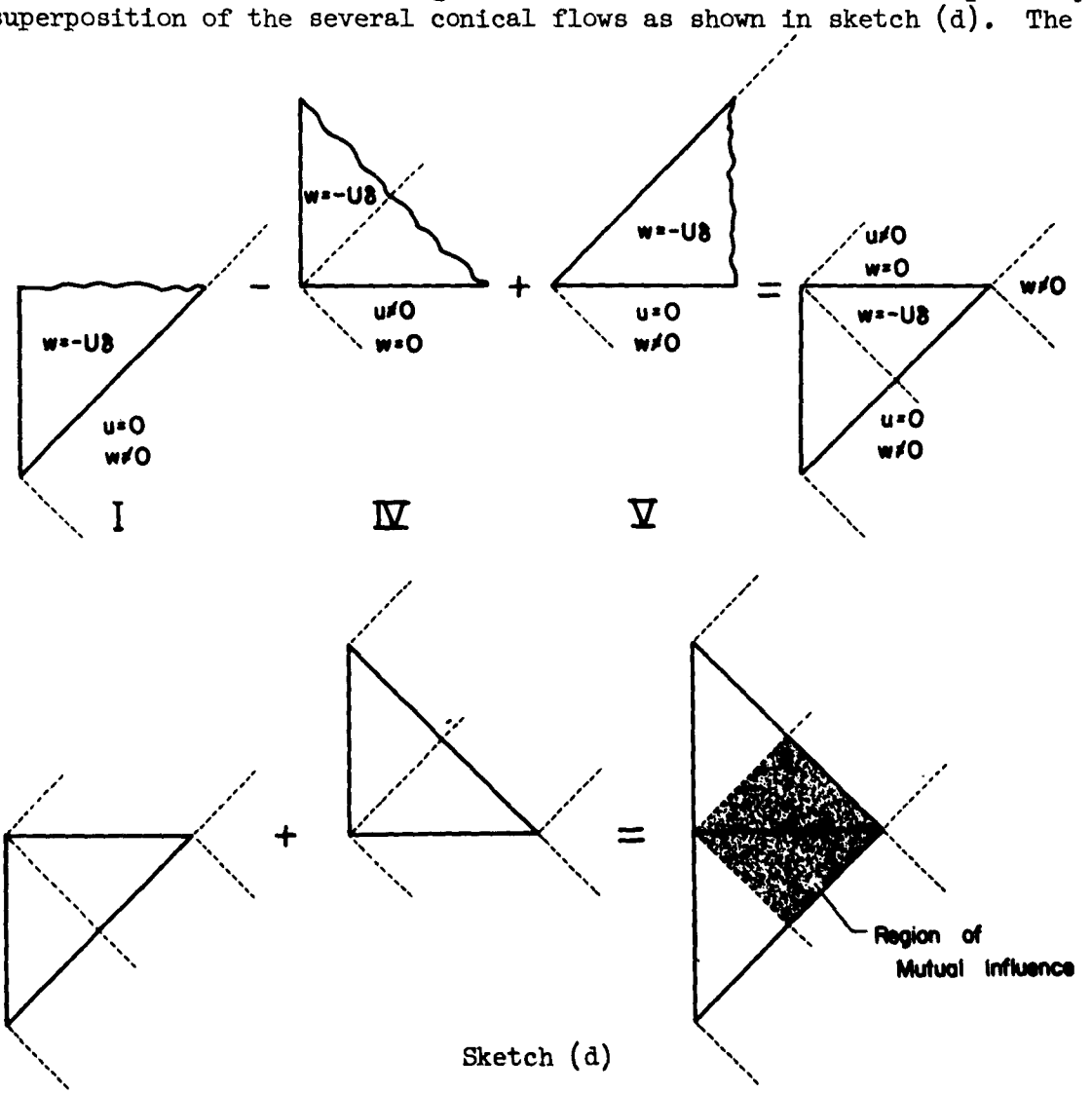

Sketch (d)

leading edge of solution V is alined with the trailing edge of solution I so that the downwash from IV is completely canceled. Solution I has already been discussed and the streamwise velocity perturbation is given by equation (5a). Solutions IV and V are given by numbers 1 and 9 of table A, 13a of reference 8. Since u_V does not influence the pressures on the fins, it will not be considered at this time.

$$u_{IV} = \mathrm{Re}\,\frac{mU\delta}{\pi\sqrt{m^2 - 1}}\cos^{-1}\frac{1 - m\tau}{m - \tau}\Bigg|_{m \to \infty} \tag{9a}$$

Upon allowing m to proceed to the limit and taking the real part

$$u_{IV} = \frac{U\delta}{\pi}\left(\frac{\pi}{2} - \tan^{-1}\frac{zy}{x^2 - z^2 + x\sqrt{x^2 - y^2 - z^2}} + 2\tan^{-1}\frac{y}{x - z + \sqrt{x^2 - y^2 - z^2}}\right) \tag{9b}$$

$$u_{IV}\Big|_{z=0} = \frac{U\delta}{\pi}\left(\frac{\pi}{2} + \sin^{-1}\frac{y}{x}\right) \tag{9c}$$

Therefore, on the surface of the fin (z = 0) the velocity perturbations are,

$u = \pm U\delta$ ahead of mutual influence region (10a)

$u = \pm\frac{2U\delta}{\pi}\sin^{-1}\frac{y}{x}$ inside of mutual influence region (10b)

By use of equations (1) and (10) the integration of the pressure over the fin surfaces can be carried out to yield the drag coefficient based on plan area plus fin area.

$$C_{D_{V\text{-}V}} = \frac{(4/\pi + 2)\delta^2 c^2}{bc + c^2} = \frac{3.2732\delta^2 c^2}{bc + c^2} \tag{11}$$

The drag factor, $C_{D_i}/\beta C_L^2$, is calculated from the results of equations (7) and (11).

Model 2 - Triangular Fins With Unswept Leading Edges and Sonic Trailing Edges; Wing With Curved Trailing Edge

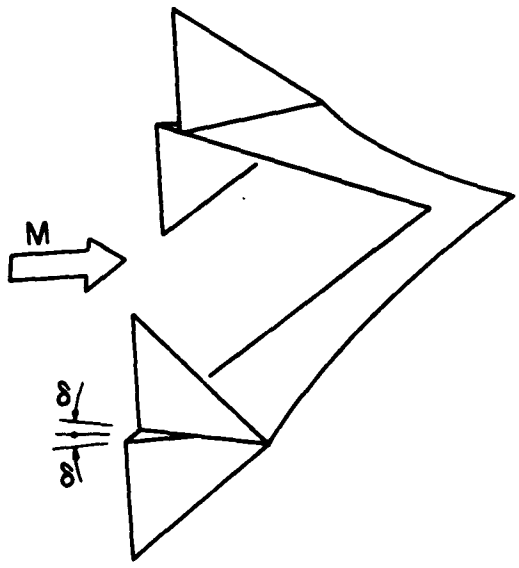

Sketch (e)

Description.- On the rear portion of the wing of Model 1, shown in sketch (a), there is a region of negative lift. In this section, the wing plan form is modified as illustrated in sketch (e) so that the trailing edge lies along the line where the local lift becomes negative. The remainder of this airfoil system is the same as Model 1.

Lift.- The equation defining the pressures on the horizontal surface of Model 2 is the same as for number 1, that is, equation (5). From this equation it is possible to find the expression for the line on the wing along which $C_p = 0$.

$$C_p = 0 = \pm 2\delta \mp \frac{4\delta}{\pi}\left(\tan^{-1}\frac{zc}{x^2 - z^2 + x\sqrt{x^2 - c^2 - z^2}} + 2\tan^{-1}\frac{z}{x - c + \sqrt{x^2 - c^2 - z^2}}\right)$$

Through the use of trigonometric relations and after some algebraic manipulations, the equation for the line on the wing along which the pressure is zero is

$$z = \sqrt{x^2 - xc} \tag{12a}$$

or

$$x = \frac{c + \sqrt{c^2 + 4z^2}}{2} \tag{12b}$$

The plan area of the wing is now found as

$$S = 2\int_0^b \left(\frac{c}{2} + \frac{1}{2}\sqrt{c^2 + 4z^2} - z\right)dz$$

$$S = cb + \frac{b}{2}\sqrt{c^2 + 4b^2} - b^2 + \frac{c^2}{4}\ln\frac{2b + \sqrt{c^2 + 4b^2}}{c} \tag{13}$$

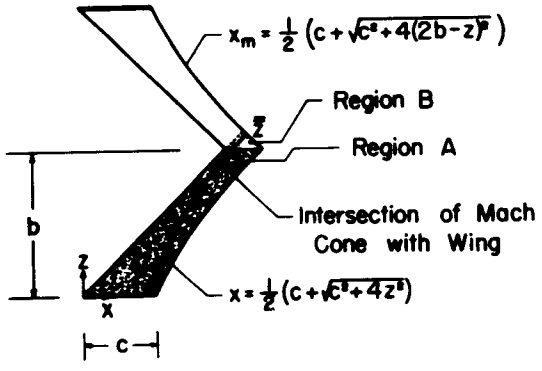

Sketch (f)

The lift is found by integrating equation (5) over the wing surface. As before, the lift is divided into two parts, A and B, as indicated in sketch (f). The coefficients are, after integration with respect to x

$$C_{L_A} = \frac{16\delta}{\pi S}\int_0^b \left[z \tan^{-1}\sqrt{\frac{\sqrt{c^2 + 4z^2} - c}{2c}} - \frac{\pi z}{2} + \frac{\pi c}{2} + z \ln \frac{c + \sqrt{c^2 + 4z^2} + \sqrt{2c(\sqrt{c^2 + 4z^2} - c)}}{2\sqrt{c^2 + z^2}} + c \sin^{-1} \frac{c(\sqrt{c^2 + 4z^2} - c) - 2z^2}{\sqrt{c^2 + z^2}(\sqrt{c^2 + 4z^2} - c)} \right] dz \tag{14a}$$

$$C_{L_B} = \frac{2}{S}\left\{ G + \frac{8\delta}{\pi}\int_b^{\bar{\bar{z}}} \left[x_m \left(\tan^{-1} \frac{zc}{x_m^2 - z^2 + x_m\sqrt{x_m^2 - c^2 - z^2}} + 2 \tan^{-1} \frac{z}{x_m - c + \sqrt{x_m^2 - c^2 - z^2}} \right) - \pi x_m + \frac{\pi c}{2} + z \tan^{-1}\sqrt{\frac{x_m^2 - c^2 - z^2}{c^2}} + z \ln \frac{x_m + \sqrt{x_m^2 - c^2 - z^2}}{\sqrt{c^2 + z^2}} + c \sin^{-1} \frac{c(x_m - c) - z^2}{\sqrt{c^2 + z^2}(x_m - c)} \right] dz \right\} \tag{14b}$$

where

$$\bar{\bar{z}} = \frac{4b(4b^2 - c^2) + 2\sqrt{2}bc\sqrt{2b^2 + c^2}}{16b^2 - c^2} \tag{15}$$

$$x_m = \frac{1}{2}\left[c + \sqrt{c^2 + 4(2b - z)^2} \right] \tag{16}$$

and G is the lift over region B when a two-dimensional pressure distribution is assumed to exist.

$$G = 2\delta\left[\frac{bc^2}{4b - c} - \left(\frac{4b^2}{4b - c}\right)^2 + b^2 + \frac{2bc - 4b^2}{2(4b - c)}\sqrt{c^2 + 4\left(2b - \frac{4b^2}{4b - c}\right)^2} + \right.$$

$$\left. \frac{b\sqrt{c^2 + 4b^2}}{2} + \frac{c^2}{4} \ln \frac{4bc - 8b^2 + (4b - c)\sqrt{c^2 + 4\left(2b - \frac{4b^2}{4b - c}\right)^2}}{(4b - c)(\sqrt{c^2 + 4b^2} - 2b)}\right] \tag{17}$$

The aspect ratio for Model 2 is,

$$A = \frac{4b^2}{S} \tag{18}$$

where S is given by equation (13).

Drag.- The pressure drag of the fins of Model 2 is the same as for Model 1. The coefficient is different because of the change in the plan area. So

$$C_{D_{v-v}} = \frac{2\left(\frac{4}{\pi} + 2\right)\delta^2 c^2}{S + 2c^2} = \frac{6.546\delta^2 c^2}{S + 2c^2} \tag{19}$$

Model 3 - Triangular Fins With Sonic Leading Edges and Unswept Trailing Edges

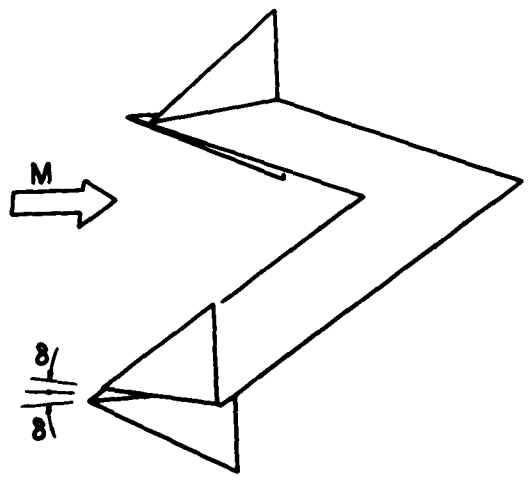

Sketch (g)

Description.- The horizontal surface of this airfoil combination is the same as number 1. The fin shape differs in that the leading edge is swept along the Mach line and the trailing edge is unswept as shown in sketch (g).

Lift.- Since all the edges of this configuration are either sonic or supersonic, the upper and lower surfaces of the wing may once again be treated independently.

The boundary condition on the fin and on the wing can be satisfied by the selection of a plane of symmetry from a particular conical flow as illustrated in sketch (h). The Mach cone from the fin tip does not intersect the horizontal surface. Therefore, the streamwise velocity perturbation in the $y = 0$ plane yields the pressure on the wing.

From number 3 of table A, 13a of reference 8, the streamwise velocity perturbation for the conical fin shown in sketch (h) is

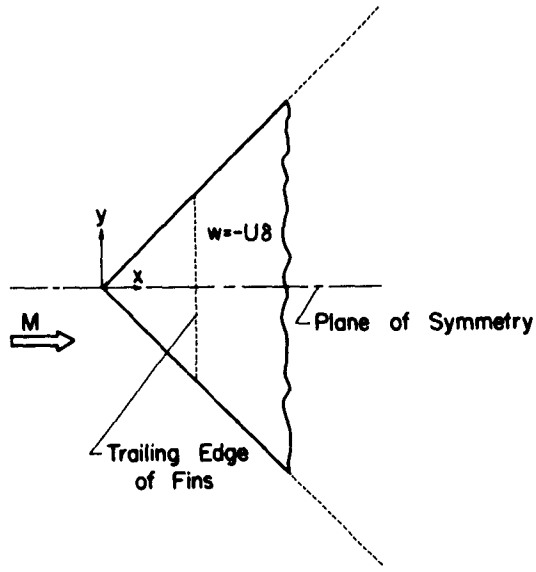

Sketch (h)

$$u_V = \mathrm{Re}\,\frac{mU\delta}{\pi\sqrt{m^2-1}}\left(\cos^{-1}\frac{1-m\tau}{m-\tau}+\cos^{-1}\frac{1+m\tau}{m+\tau}\right)\Bigg|_{m\to 1}$$

After m has proceeded to the limit and the real part is taken through the use of equation (4),

$$u_V = \frac{2U\delta}{\pi}\,\frac{(x^2-z^2+x\sqrt{x^2-y^2-z^2})(x^2-y^2+x\sqrt{x^2-y^2-z^2})-z^2y^2}{(x^2-y^2+x\sqrt{x^2-y^2-z^2})^2+z^2y^2} \tag{20}$$

On the top of the wing, $y = 0$,

$$C_p = -\frac{2u}{U} = -\frac{4\delta}{\pi}\,\frac{\sqrt{x^2-z^2}}{x} \tag{21}$$

As was done with the previous models, the lift is divided into two parts, A and B, part A being direct lift and B the overlap lift (sketch (i)). The lift for these two parts is integrated and found as

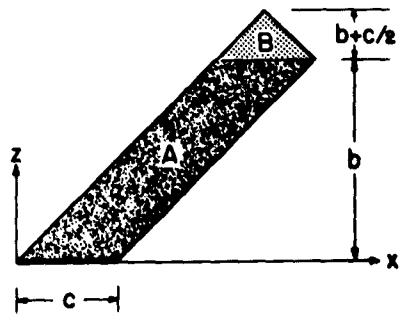

Sketch (i)

$$C_{L_A} = \frac{8\delta}{\pi(bc + c^2)} \left[\sqrt{2bc + c^2} \left(\frac{3}{2} b + c \right) + \frac{b^2}{2} \left(\frac{\pi}{2} - \sin^{-1} \frac{b}{b + c} \right) - \right.$$

$$\left. (2b + c)^2 \cot^{-1} \sqrt{\frac{2b + c}{c}} \right] \tag{22a}$$

$$C_{L_B} = \frac{8\delta}{\pi(bc + c^2)} \left\{ \frac{1}{3c} \left[(2bc + c^2)^{3/2} - c^3 \right] + \frac{b^2}{2} \left(\sin^{-1} \frac{b}{b + c} - \frac{\pi}{2} \right) + \right.$$

$$\left. \frac{4c - b}{6} \sqrt{2bc + c^2} - \frac{c^2}{2} \left(\frac{4}{3} + \frac{\pi}{2} \right) + c^2 \tan^{-1} \sqrt{\frac{c}{2b + c}} \right\} \tag{22b}$$

Drag.- The pressure on the inside of the fin surfaces can be calculated from equation (21) by setting $z = 0$. On the outside surfaces, the upper and lower fins interfere on each other in such a way as to reduce their drag. The pressures on these surfaces could be found and integrated for the drag. This procedure is not necessary because the drag can be found directly from the results of the previous sections through the use of reverse-flow theorems. Inspection of sketches (a) and (g) shows that the fins are identical if the flow direction over one of them is reversed. Within the linearized approximation being used in this report, the drag of the two fin plan forms is the same in forward and reverse flow as demonstrated in references 12 and 13. Therefore, the drag coefficient for this wing-fin combination is also given by equation (11).

Model 4 - Trapezoidal Fins on a Swept Wing

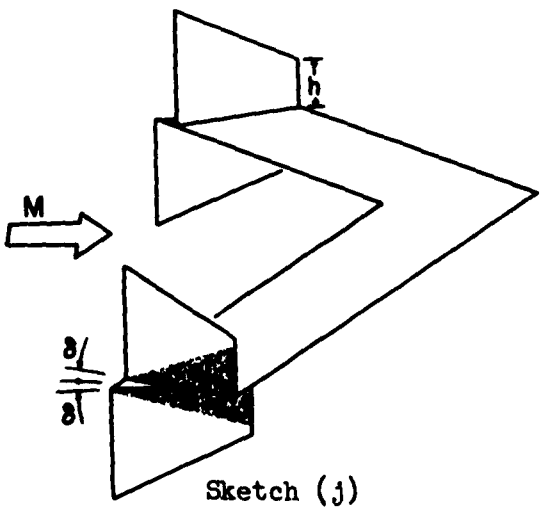

Sketch (j)

Description.- The three previous models have fins which are only of the order of one chord length high. Consider now the case when the triangular fin is raised and a rectangular section is added as shown in sketch (j). The upper and lower fins are deflected differentially to give a positive lift. All edges of the fins are unswept except the fin tip, which is swept along the Mach line.

Lift and drag.- The fins are assumed to be high enough so that the Mach cones from the tips do not intersect the wing. The minimum height, h,

of the rectangular section which affords this condition is found by seeking the point where the Mach cone from the fin tip first intersects the wing. The equation for the intersection of the Mach cone with the plane of the wing is,

$$x^2 = (c + h)^2 + z^2$$

when the Mach cone first makes contact with the wing trailing edge, $x = c + z$ (sketch (k)). Substituting this in the above equation

$$z = h + \frac{h^2}{2c} \equiv z_h \qquad (23)$$

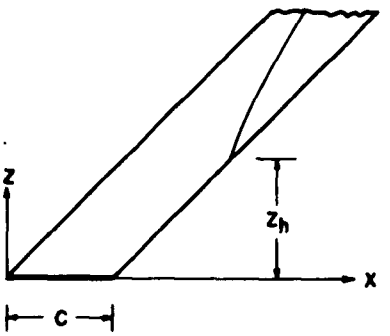

Sketch (k)

If the fin is high enough so that $z_h \geq b$ and $h \geq c$, the lift and drag coefficients based on plan form plus fin area are,

$$C_{L_{V-h}} = \frac{4\delta bc + \frac{c^2}{4} 4\delta}{bc + c^2 + 2hc} \qquad (24a)$$

$$C_{D_{V-V}} = \frac{4\delta^2(2hc + c^2) - \frac{4}{\pi} \delta^2 c^2}{bc + c^2 + 2hc} \qquad (24b)$$

The second term in the numerator of the lift coefficient is the lift contribution from the doubling-up effect at and near the center of the wing. The second term in the numerator of the drag coefficient is the reduction in drag due to the mutual interference of pressure fields of the upper and lower fins in the region indicated by the shaded area in sketch (j).

Model 5 - Wing and Fins in Horizontal Plane

Description.- The question may be asked whether it might not be profitable to lean the fins outward with respect to the wing as illustrated in a front view of sketch (l).

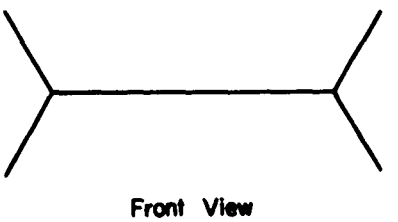

Front View

Sketch (l)

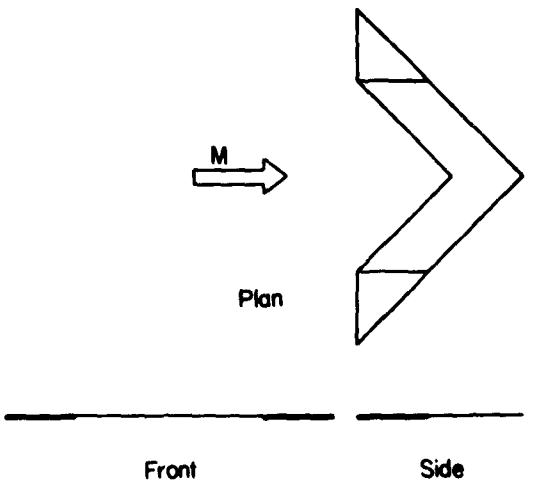

Sketch (m)

The general case is difficult to evaluate because of the superpositions involved. However, the limiting case of the fins and wing in the horizontal plane, sketch (m), is simple to analyze. The fins (one on each wing tip) are deflected so that they not only induce lift on the wing, which is at $\alpha = 0$, but carry lift themselves.

Lift and drag.- The pressures on the fins and wing are given by equation (9c). The integration of these pressures for lift and drag in the various regions is carried out.

$$C_L = \frac{2\delta}{bc + \frac{c^2}{2}} \left\{ (bc + c^2) + \frac{2}{\pi} \left[b^2 \sin^{-1} \frac{b}{b + c} + 2(c^2 + 2bc + 2b^2) \left(\frac{\pi}{2} - \tan^{-1} \sqrt{\frac{2b + c}{c}} \right) - \frac{\pi}{2} (b^2 + bc + c^2) - b\sqrt{2bc + c^2} \right] \right\} \quad (25)$$

$$C_{D_i} = \frac{\left(1 + \frac{2}{\pi}\right)\delta^2 c^2}{bc + \frac{c^2}{2}} = \frac{1.637\delta^2 c^2}{bc + \frac{c^2}{2}} \quad (26)$$

The aspect ratio is given by

$$A = \frac{(2b + 2c)^2}{(2b + c)c} \quad (27)$$

Optimum Deflection of Wing

Description.- In the airfoil combinations studied so far, the wing has been undeflected. It is therefore not being utilized to the best advantage. In order to obtain the highest efficiency from the wing, it should be deflected so that the drag factor $C_{D_i}/\beta C_L^2$ is brought to a

minimum. This minimum is derived by finding an optimum ratio, $\sigma = \alpha/\delta$, between the wing angle of attack and the fin deflection. When both the wing and fins are deflected, the drag factor may be written as

$$\frac{C_{D_i}}{C_L^2} = \frac{\sigma\left(\sigma C'_{L_{h-h}} + C'_{L_{v-h}}\right) + C''_{D_{v-v}} + \sigma C''_{D_{h-v}} - \sigma^2 C''_{D_t}}{\left(\sigma C'_{L_{h-h}} + C'_{L_{v-h}}\right)^2} \tag{28}$$

The primes in equation (28) signify derivatives with respect to the deflection angle of the various surfaces. Note that there is a contribution to the drag arising from lift induced by the fins on the now deflected horizontal surface.[3] Differentiating equation (28) with respect to σ while holding all the coefficients constant and then setting the result equal to zero furnishes the maximums and minimums of the C_{D_i}/C_L^2 versus σ curve. Two values of σ are found: When C_{D_i}/C_L^2 is a maximum, that is, not an optimum,

$$\sigma = -\frac{C'_{L_{v-h}}}{C'_{L_{h-h}}}, \qquad \frac{C_{D_i}}{C_L^2} = \infty$$

and when C_{D_i}/C_L^2 is a minimum, an optimum,

$$\sigma = \frac{2C'_{L_{h-h}}C''_{D_{v-v}} - C'_{L_{v-h}}\left(C'_{L_{v-h}} + C''_{D_{h-v}}\right)}{C'_{L_{h-h}}\left(C'_{L_{v-h}} - C''_{D_{h-v}} - 2\dfrac{C'_{L_{v-h}}}{C'_{L_{h-h}}}C''_{D_t}\right)} \tag{29}$$

The first value of σ defines the ratio in which the fins and wing should be deflected to yield zero lift; that is, it defines how the wing is to lift an amount equal and opposite to the lift induced by the fins. Therefore, the model has drag without lift and the drag factor becomes infinite.

The optimum value of σ defines the ratio in which the fins and wing should be deflected to give the most lift for the drag. In general, σ is positive, indicating that both the fins and the wing lift contributions are in the same direction. Hereafter, the term σ will be used to denote only the value which yields the optimum ratio.

[3]Considerations of this type must be taken into account when thickness of the various surfaces is considered.

Equation (29) could be applied to all of the airfoil combinations studied so far except number 5. It is applied to Models 1, 2, and 3, but not to 4. Before this is done, it is first necessary to find $C_{L_{h-h}}$, the lift on the wing when it is deflected, and the drag $C_{D_{h-v}}$ induced on the fins by the wing. Since all the edges are either sonic or supersonic, none of the surfaces have leading-edge suction and therefore C_{D_t} is zero for these three cases.

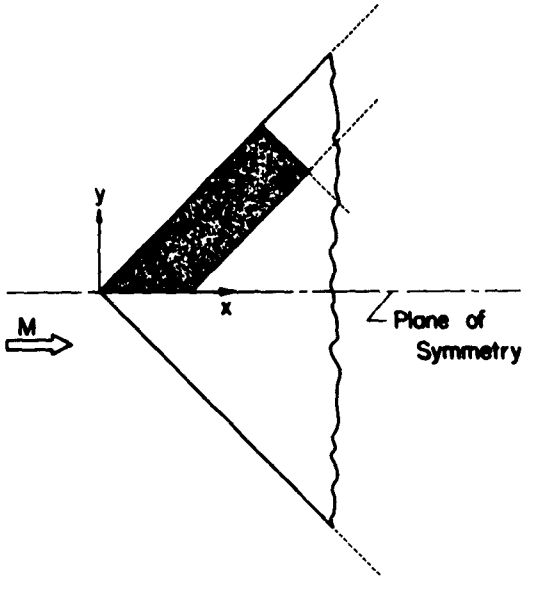

Sketch (n)

Lift of finned wing.- The pressures on the wing of Models 1 and 3 are found from a superposition of several conical flow fields. It will be assumed here that the fins are undeflected and serve merely as barriers or reflection planes. It then remains to choose a symmetrical flow field from which the parts can be dissected. A flow field of this type is given by number 3 of table A, 13a of reference 8. The streamwise perturbation velocity has already been given in equation (20). The conical-flow plan form and the part of the flow field to be used is shown in sketch (n). The manner in which the wing flow field is constructed is shown in sketch (o). The streamwise velocity perturbation on the wing is found by setting $z = 0$ in equation (20).

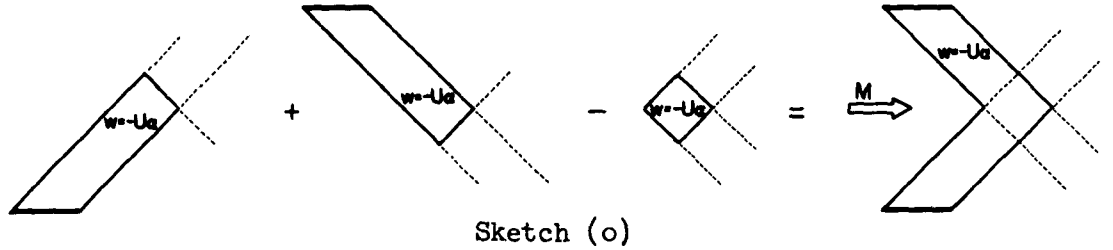

Sketch (o)

$$u\big|_{z=0} = \frac{2Ua}{\pi} \frac{x}{\sqrt{x^2 - y^2}} \tag{30}$$

By use of equations (1) and (30), the lift of the finned wing is found by integrating the pressures over the various surfaces shown in sketch (o).

$$C_{L_{h-h}} = \frac{8a}{3\pi} \frac{2(b + c)\sqrt{2bc + c^2} - 2c^2}{bc + c^2} \tag{31a}$$

for Models 1 and 3. For both models the drag is simply,

$$C_{D_{h-h}} = \alpha C_{L_{h-h}} \tag{31b}$$

The plan form of the wing for Model 2 is different from 1 and 3 but the same expression for the pressure is used. The limits of integration for the lift in this case are not so simple as for Models 1 and 3. Therefore, the spanwise integration is carried out numerically. The same superposition technique shown in sketch (o) is used for the wing with the curved trailing edges (still supersonic), and the lift is found as

$$C_{L_{h-h}} = \frac{16\alpha}{\pi S}\left\{\int_0^b \sqrt{\left(\frac{c + \sqrt{c^2 + 4y^2}}{2}\right)^2 - y^2}\, dy + \right.$$

$$\int_0^{\frac{4b^2}{4b-c}} \sqrt{\left[\frac{c + \sqrt{c^2 + 4(2b - y)^2}}{2}\right]^2 - y^2}\, dy +$$

$$\left.\int_0^{\frac{4b^2}{4b-c} - b} \sqrt{\left[\frac{c + \sqrt{c^2 + 4(b - y)^2}}{2} - b\right]^2 - y^2}\, dy\right\} \tag{32}$$

where S is defined by equation (13). The values computed by equation (32) are used in the optimum case of airfoil system 2 and are not shown in figure 2.

Interference of wing on fins.- Heretofore, when the lift from one surface was considered, the other surface was assumed to be undeflected. If both are deflected simultaneously, drag contributions will arise due to one surface interfering on another. As already pointed out, the lift induced by the fins on the wing contributes to the drag as $\delta\sigma C'_{L_{v-h}}$. The other cross inteference arises from the wing interfering on the deflected fins, designated in equation (28) as $C''_{D_{h-v}}$.

The pressures induced on the fins by the wing are given by equation (21). The region on the inside of the fins over which the pressures act is shown for the various configurations in sketch (p). After integration of equation (21) over these areas, the interfering drag is

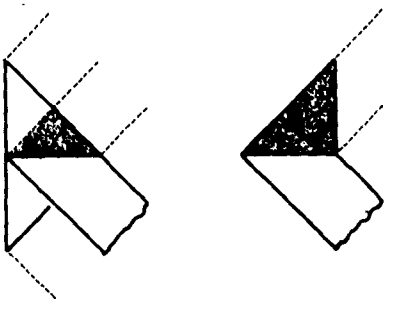

Sketch (p)

Model 1:

$$C_{D_{h-v}} = \frac{2\left(\frac{4}{\pi} - 1\right)\alpha\delta c^2}{bc + c^2} = \frac{0.546\alpha\delta c^2}{bc + c^2} \tag{33a}$$

Model 2:

$$C_{D_{h-v}} = \frac{4\left(\frac{4}{\pi} - 1\right)\alpha\delta c^2}{S} = \frac{1.093\alpha\delta c^2}{S} \tag{33b}$$

Model 3:

$$C_{D_{h-v}} = \frac{\alpha\delta c^2}{bc + c^2} \tag{33c}$$

With all the factors in equation (28) now known, the optimum relative deflection angles and the drag factor are found.

ANALYSIS OF AIRFOIL COMBINATIONS WITH FUSELAGES

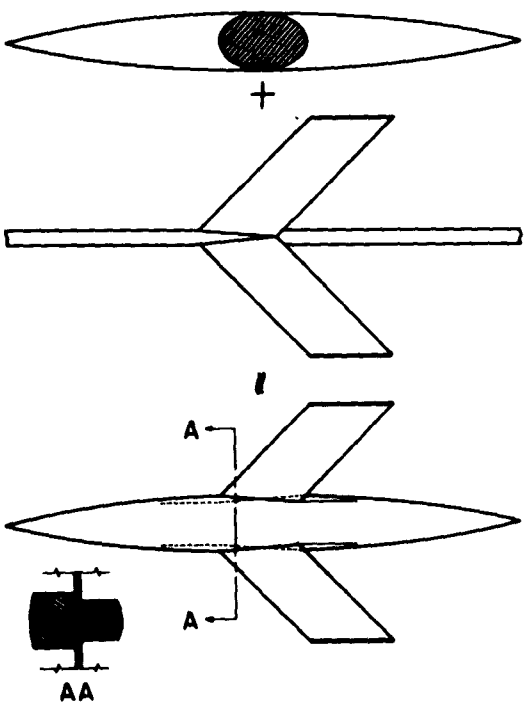

Sketch (q)

The same principles that were applied to the airfoil systems in the last section may be used in contouring the fuselages of aircraft. Several of these models are now described and analyzed. The fuselage is treated as thin in cross section and, in general, semi-infinite in length. These thin bodies which are tall in comparison with their width, are thought of as perturbations on the fuselage shape to be used in a design, as indicated in sketch (q). If the fuselage is slender (maximum diameter approximately equal to height of perturbation body), this method of treating the problem is not believed to affect greatly the efficiency of the configuration.

Model 6 - Triangular Fins With Unswept Leading Edges and Sonic Trailing Edges

Description.- An examination of the streamline paths over the wing of Model 1 as indicated in plan view of sketch (r), reveals one criterion for contouring the fuselage. If a slender body is placed along the center line of the model, the part on top of the wing must increase and the part on the bottom must decrease in width to follow the streamlines. These lateral perturbations which would be required on a conventional body are illustrated in sketch (s). The pressures induced by the fins exert a thrust on this new contour. The paths of the streamlines and thrust on the body will now be calculated.

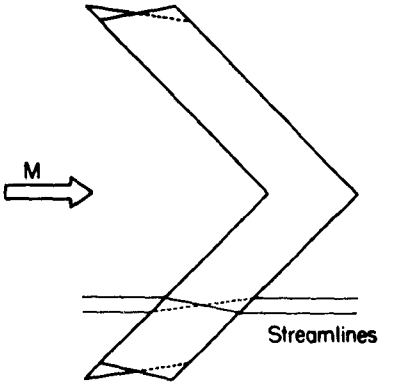

Sketch (r)

Thrust on fuselage due to fin deflection.- For simplicity of calculation the body is assumed to lie in the $z = b$ plane. The local pressures on the fuselage are given by equations (5). Since $u_I \neq u_{II}$, at all points on the body, a separate expression must be written for the pressure in each of the three regions shown in sketch (t). Region 1 includes that part of the fuselage which feels the full induced pressure of the fins but does not realize that the fins are finite in extent. In region 2, the pressures are decreasing in the stream direction because the tips of the fins are relieving the pressure more and more. The boundary of region 2 is defined by the intersection of the fin-tip Mach cones on the fuselage and the reflection of these Mach cones from the wing surface. In region 3 the pressures decrease still further. This reflection effect is analyzed by placing an image fin below the wing.

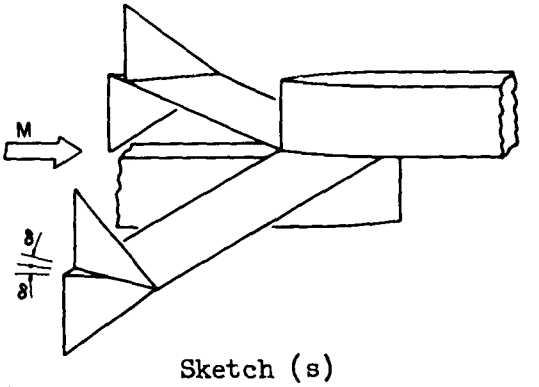

Sketch (s)

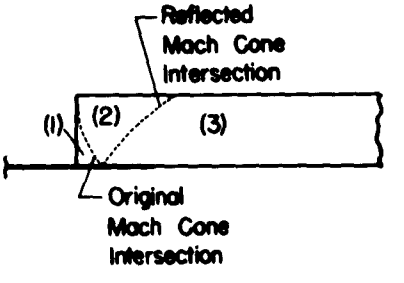

Sketch (t)

The pressure induced by the fins in each of the three regions on the upper body are

Region 1:

$$C_p = -2\delta \tag{34a}$$

Region 2:

$$C_p = -\frac{2\delta}{\pi}\left(\tan^{-1}\frac{by}{x^2-b^2+x\sqrt{x^2-y^2-b^2}}+2\tan^{-1}\frac{b}{x-y+\sqrt{x^2-y^2-b^2}}\right) \tag{34b}$$

Region 3:

$$C_p = -\frac{2\delta}{\pi}\left[\tan^{-1}\frac{by}{x^2-b^2+x\sqrt{x^2-y^2-b^2}}+2\tan^{-1}\frac{b}{x-y+\sqrt{x^2-y^2-b^2}}+\right.$$

$$\left.\tan^{-1}\frac{b(2c-y)}{x^2-b^2+x\sqrt{x^2-(2c-y)^2-b^2}}+2\tan^{-1}\frac{b}{x+y-2c+\sqrt{x^2-(2c-y)^2-b^2}}\right]+2\delta \tag{34c}$$

The thrust on both sides of the upper fuselage may be written approximately as

$$\frac{T}{q} = 2\int_o^c\int_b^{b+c} C_p\,\frac{w}{U}\,dx\,dy \tag{35}$$

where $w/U = dz/dx$ and the equations for the pressure and slope change as the integration proceeds over the various regions.

The slope of the body, or streamlines in the $z = b$ plane, is found by substituting the proper limits into solution number 9 of table A, 13a of reference 8.

$$w_I = \mathrm{Re}\,\frac{2U\delta}{\pi}\left[\sqrt{\frac{m_2-m_1}{m_1(m_2+1)}}\,\sinh^{-1}\sqrt{\frac{m_1-\tau}{(1+m_1)\tau}}-\tan^{-1}\sqrt{\frac{(m_2-m_1)(1+\tau)}{(m_2+1)(m_1-\tau)}}\right]_{\substack{m_1\to 1\\ m_2\to\infty}} \tag{36}$$

After the limits are inserted and the real part is taken through the use of equation (4)

$$\left(\frac{w}{U}\right)_I = \frac{\delta}{\pi}\left(\frac{1}{2}\ln\frac{x+\sqrt{x^2-y^2-z^2}}{x-\sqrt{x^2-y^2-z^2}}+\tan^{-1}\frac{x-y+z+\sqrt{x^2-y^2-z^2}}{x+y+z+\sqrt{x^2-y^2-z^2}}+\tan^{-1}\frac{x-y-z+\sqrt{x^2-y^2-z^2}}{x+y-z+\sqrt{x^2-y^2-z^2}}-\pi\right) \tag{37}$$

The slope of the body in each of the three regions shown in sketch (t) is then

Region 1:

$$\frac{w}{U} = \delta \tag{38a}$$

Region 2:

$$\frac{w}{U} = \left(\frac{w}{U}\right)_I\Bigg|_{z=b} \tag{38b}$$

Region 3:

$$\frac{w}{U} = \left(\frac{w}{U}\right)_I\Bigg|_{z=b} + \frac{\delta}{\pi}\left[\frac{1}{2}\ln\frac{x+\sqrt{x^2-(2c-y)^2-b^2}}{x-\sqrt{x^2-(2c-y)^2-b^2}} + \tan^{-1}\frac{x+y-2c+b+\sqrt{x^2-(2c-y)^2-b^2}}{x-y+2c+b+\sqrt{x^2-(2c-y)^2-b^2}} + \right.$$

$$\left. \tan^{-1}\frac{x+y-2c-b+\sqrt{x^2-(2c-y)^2-b^2}}{x-y+2c-b+\sqrt{x^2-(2c-y)^2-b^2}}\right] \tag{38c}$$

The complexity of equations (34) and (38) necessitates the integration of equation (35) by graphical means. The local pressure, slope, and hence thrust are calculated at various points on the fuselage. These local thrust values are then plotted and integrated for total thrust. The thrust on the lower part of the fuselage is the same as that on the upper part so only one integration is necessary. Typical values of slope, pressure, and thrust for the upper body are shown in figure 5 for $b/c = 1$. Note that negative values arise in region 3. All integrations are stopped when the pressure or slope on the body changes sign. The final integrated values of the thrust are shown in figure 6.

The equation for the slope of the fuselage can be integrated to yield the coordinates of the fuselage shape. Since $w/U = dz/dx$ and because the z variations are assumed to be small, z may be set equal to b for the integration of equation (37).

Region 1, $x \leq \sqrt{y^2+b^2}$:

$$z = \delta(x-b) \tag{39a}$$

Region 2, $x \geq \sqrt{y^2+b^2}$:

$$z = \frac{\delta}{\pi}\left[\pi(b-x) + \frac{x}{2}\ln\frac{x+\sqrt{x^2-y^2-b^2}}{x-\sqrt{x^2-y^2-b^2}} - \sqrt{x^2-y^2-b^2} + y\ln\frac{\sqrt{y^2+b^2}}{x+\sqrt{x^2-y^2-b^2}} + \right.$$

$$b\tan^{-1}\frac{xy}{b\sqrt{x^2-y^2-b^2}} - \frac{\pi b}{2} + x\tan^{-1}\frac{x-y+b+\sqrt{x^2-y^2-b^2}}{x+y+b+\sqrt{x^2-y^2-b^2}} +$$

$$\left. x\tan^{-1}\frac{x-y-b+\sqrt{x^2-y^2-b^2}}{x+y-b+\sqrt{x^2-y^2-b^2}}\right] \qquad (39b)$$

The coordinates of the body in region 3 are given by an equation which is equivalent to equation (39b) plus similar terms to account for the reflected Mach cone interference.

Thrust on fuselage due to fin and wing deflection.- When the wing is deflected in combination with the fins, pressures are induced by the wing which also exert a thrust on the fuselage. The thrust on the perturbation body is expressed as the integral of the product of the slope induced by the fins and the pressure induced by the wing over the fuselage sides. This thrust augments that due to the fin interference.

From equation (20) the pressure on the fuselage induced by the wing is

$$C_p = \frac{-4\alpha}{\pi}\frac{\left[x^2-(y-c)^2+x\sqrt{x^2-(y-c)^2-b^2}\right]\left[x^2-b^2+x\sqrt{x^2-(y-c)^2-b^2}\right]-(y-c)^2b^2}{\left[x^2-b^2+x\sqrt{x^2-(y-c)^2-b^2}\right]^2+(y-c)^2b^2} \qquad (40)$$

where the change in coordinates has been incorporated so that equations (38) and (40) correspond to the same coordinate system. As before, the integration is carried out graphically. The results of this integration are shown in figure 6. The thrust coefficient based on plan form plus fin area is shown in figure 4(b) along with the drag coefficient of some of the other models discussed. The thrust coefficient for the fin interference on the body and for the wing interference on the body is represented by $-C_{D_{v-b}}$ and $-C_{D_{h-b}}$, respectively.

The lift and drag for Model 6 is given by equations (7a) and (11) when only the fins are deflected. The overlap lift given by equation (7b) has been eliminated. The optimum combination is found by equations (28) and (29) along with (31) for the horizontal-surface values.

Throughout the analysis of the thrust of this wing-body combination it is assumed that the slope of the sides of the perturbation fuselage deviate from the vertical by a negligible amount.

Model 7 - Triangular Fins With Unswept Leading Edges and Sonic Trailing Edges; Wing With Curved Trailing Edge

Description.- This model, sketch (u), is the same as Model 6 with the exception that that portion of the wing has been removed which contributes negative lift, as already discussed for Model 2. The forces on the various components are found from the relations already developed. The thrust and shape of this fuselage are the same as Model 6 because the integration is stopped when the pressure becomes negative, or at the trailing edge in this case. The lift is found from the results of Model 2.

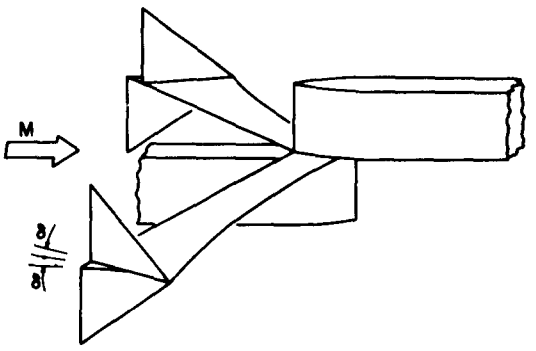

Sketch (u)

Model 8 - Positive and Negative Wedge Superimposed on Fuselage

Description.- The pressure waves were cast out over the wing by the fin in the last group. The same effect could be obtained by contouring the fuselage to do this. Such a perturbation model is shown in sketch (v). The sides of the perturbation body are flat rectangular surfaces which are deflected. The wing end plates are not deflected in this case. A more efficient combination could probably be obtained by deflecting them the proper amount.[4]

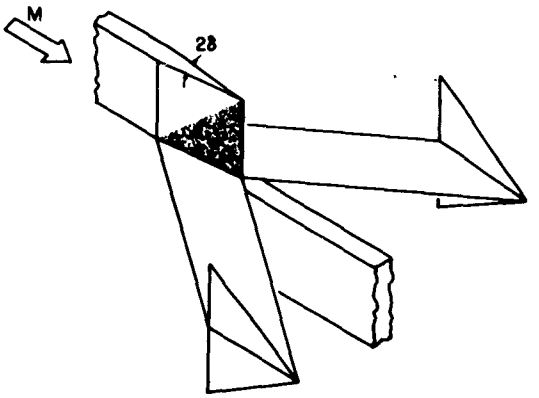

Sketch (v)

[4]The fins need not be on the wing. In this case the calculations are simplified in the tip region and the model is completed by the addition of control surfaces. In a design, the end plates may be replaced by external stores which are contoured to follow the curvature of the streamlines induced by the fuselage. The external stores would then receive a thrust from the wing and fuselage interference similar to Models 6 and 7.

Lift.- The lift is divided into two parts: that due to the fuselage contour and that due to the wing deflection. The lift and drag generated by the wing deflection are given by equation (31). The indirect lift induced by the fuselage contour on the wing is calculated by the same method used for the other cases. The general equation for the basic conical flow is obtained from solution 1 of table A, 13a of reference 8. The streamwise perturbation velocity for this conical flow is given by equation (9b). The pressure induced on the top of the wing by the fuselage is then

$$C_p = -\frac{2u}{U} = -2\left(2\frac{u_{IV}}{U} - \delta\right)$$

$$C_p = -\frac{4\delta}{\pi}\left(2\tan^{-1}\frac{c}{x-z+\sqrt{x^2-c^2-z^2}} - \tan^{-1}\frac{zc}{x^2-z^2+x\sqrt{x^2-c^2-z^2}}\right) \tag{41}$$

The indirect lift on the wing is found by integrating equation (41) over the wing surface. It must be noted that the pressure waves generated by the fuselage are reflected by the fin at the wing tips, resulting in a doubling up of the lift in this region. After performing the integration with respect to x, the lift in the two regions is

$$C_{L_A} = \frac{8\delta}{\pi(bc+c^2)}\int_o^b \left\{(z+c)\left[2\tan^{-1}\frac{c}{c+\sqrt{2cz}} - \tan^{-1}\frac{zc}{zc+(z+c)(c+\sqrt{2cz})}\right] + c\ln\frac{c+z+\sqrt{2cz}}{\sqrt{c^2+z^2}} + z\sin^{-1}\frac{z-c}{\sqrt{c^2+z^2}} - \frac{\pi z}{2} + z\tan^{-1}\sqrt{\frac{c}{2z}}\right\} dz \tag{42a}$$

$$C_{L_B} = \frac{1}{cb+c^2}\left(\delta c^2 + \frac{8\delta}{\pi}\int_b^{\bar{z}}\left\{\frac{\pi}{2}\left[2z-(2b+c)\right] + c\ln\frac{2b+c-z+\sqrt{(2b+c)^2-2z(2b+c)-c^2}}{\sqrt{c^2+z^2}} + (2b-z+c)\left[2\tan^{-1}\frac{c}{2b+c-2z+\sqrt{(2b+c)^2-2z(2b+c)-c^2}} - \tan^{-1}\frac{zc}{(2b+c)^2-2z(2b+c)+(2b+c-z)\sqrt{(2b+c)^2-2z(2b+c)-c^2}}\right] - z\tan^{-1}\frac{\sqrt{(2b+c)^2-2z(2b+c)^2-c^2}}{c} + z\sin^{-1}\frac{z(2b+c-2z)-c^2}{\sqrt{c^2+z^2(2b+c-2z)}}\right\} dz\right) \tag{42b}$$

where $\bar{z}$ is defined in equation (6c).

Drag.- In this case, the fins do not contribute to the drag because they are undeflected and of zero thickness. The deflected plates on the body sides have a drag contribution from both their own deflection and the interference of the wing on them. The direct drag is found by integration of the pressure as given by equation (9c) over the surfaces on the body.

$$C_{D_{v-v}} = \frac{\delta^2 c}{b + c}\left(4 - \frac{2}{\pi}\right) = 3.36\,\frac{\delta^2 c}{b + c} \tag{43a}$$

The drag arising indirectly from the interference of the wing on the body is found by integrating equation (21) over the area on the body influenced by the wing, as indicated by the crosshatched area in the side view in sketch (v).

$$C_{D_{h-v}} = \frac{\delta\alpha c}{b + c} \tag{43b}$$

Model 9 - Positive and Negative Wedge Superimposed on Fuselage; Subsonic Leading-Edge Wing

Description.- The wings with sonic leading edges considered so far are not so efficient as some other plan forms. In an attempt to ascertain the effect of wing plan form on the efficiency of these special models, a more efficient wing is considered. The combination consists of a contoured fuselage and a wing with subsonic leading edges and sonic trailing edges. (See sketch (w).) The trailing edge is taken to be sonic in order to simplify the geometry and the calculations. The taper ratio of the wing is 1/4. The streamwise length of the rectangular sections on the fuselage are only long enough so that their influence does not reach the leading edge or extend past the trailing edge. This streamwise length is then equal to the root chord of the wing times the taper ratio.

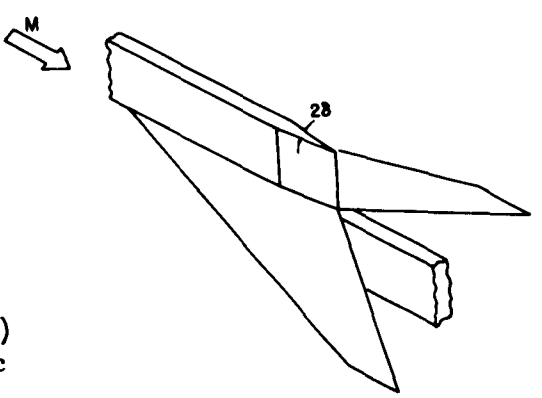

Sketch (w)

Both the wing and wedge are assumed to be deflected in the optimum ratio which is defined by equation (29).

Lift.- The lift generated by deflection of the wing is read directly from figure 10 of reference 14. For the range of aspect ratios considered

the lift induced by the body sections is calculated by equation (42a), where b and the area of the wing are adjusted to this configuration. The loss in lift generated by the wedge in the region of the wing tip Mach cone is neglected. The final result would probably not be changed by taking this into account.

Drag.- Drag contributions arise from the wing deflection, wing leading-edge thrust, wing interference on the fuselage, and from the deflected sides of the fuselage. The drag component due to the wing deflection is simply $\alpha C_{L_{h-h}}$. The leading-edge thrust is calculated in the usual manner (see, e.g., p. 219 of ref. 15). The drag of the side plates is found from equation (43) with the denominator adjusted to the proper area. The expression for the pressure acting on the body due to wing interference is found from number 6 of table A, 13a of reference 8, as

$$u = \mathrm{Re}\,\frac{m^2 U\alpha}{E(\sqrt{1 - m^2})}\,\frac{1}{\sqrt{m^2 - \tau^2}} \tag{44}$$

where $E(\sqrt{1 - m^2})$ is the complete elliptic integral of the second kind (see ref. 16). The real part of equation (44) is found through the use of equation (4) and the pressure on the body is,

$$(C_p)_{y=o} = \frac{2\alpha\sqrt{x^2 - z^2}\,\cot^2\Lambda}{E(\sqrt{1 - \cot^2\Lambda})\sqrt{z^2(1 - \cot^2\Lambda) + x^2\cot^2\Lambda}} \tag{45}$$

where the coordinate system and the area of integration are shown in sketch (x). This expression is integrated graphically with respect to z.

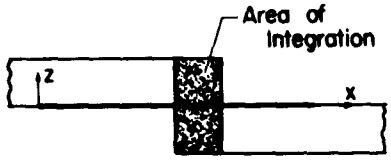

Sketch (x)

Model 10 - Half-Cone Mounted Under a Swept Wing

Description.- So far the shapes used to generate a pressure field on the wing have been flat plates. Any shape whatever may be used to generate this interfering pressure field. One such example is one half of a body of revolution mounted on the bottom of a wing. The flow is then axially symmetric and the model can be readily analyzed. A convenient choice which is relatively easy to calculate is the model wherein one half of a cone is placed under a swept wing as shown in sketch (y). The wing leading and

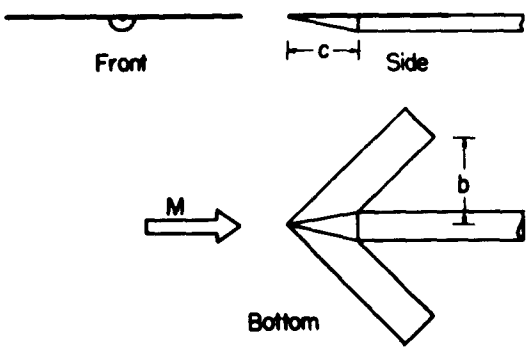

Sketch (y)

trailing edges and the wing tip are swept along the Mach line. The wing may go to angle of attack as in previous cases. The cone is assumed to be slender and to rotate with the wing so that the boundary conditions on the wing and cone are not violated.

Lift.- The lift on the wing arising from the deflection of the wing is found from equation (30). Equation (31) cannot be used because it has the negative lift contribution of the third plan form shown in sketch (o). The lift for this wing is, after integration of the pressure over the plan form shown in the bottom view in sketch (y),

$$C_{L_{h-h}} = \frac{8\alpha}{3\pi}\left[\frac{2(b+c)\sqrt{2bc+c^2}-c^2}{bc+c^2}\right] \tag{46}$$

The lift generated by the cone interaction on the wing is found by integrating the pressure induced on the wing by the cone. The linearized pressures on the wing are given by (see, e.g., ch. 4, ref. 15)

$$C_p = -\left(\frac{2u}{U}+\frac{v^2+w^2}{U^2}\right)$$

$$C_p = -\delta^2\left[\frac{\delta^2(x^2-\beta^2r^2)}{r^2} - 2\cosh^{-1}\frac{x}{\beta r}\right] \tag{47}$$

where δ is the tangent of the cone half-angle. Upon integration of equation (47) over the bottom of the wing, the lift induced by the cone is, for $\beta = 1$,

$$C_{L_{c-h}} = \frac{2\delta^2c^2}{2bc+c^2}\left[3\delta\cosh^{-1}\frac{1}{\delta} - \frac{3\delta}{2} + \frac{3\delta^3}{2} - \frac{\delta^4}{3} - \delta\sqrt{1-\delta^2} - \left(1+\frac{\delta}{3}\right)\left(\sqrt{2\delta+1}\right) - \right.$$

$$\delta(\delta+2)\cosh^{-1}\frac{\delta+1}{\delta} + \frac{\delta^2c}{3b} - \delta^2\ln\frac{b}{\delta c} + 2\left(\frac{b+c}{c^2}\sqrt{2bc+c^2}\right) +$$

$$\left.\delta^2\left(\frac{2b+c}{c}\right)^2\ln\frac{2b+c}{2b} - \delta^2\left(\frac{2c+b}{6b}\right)\left(\frac{2b+c}{c}\right)^2 + \frac{2\delta^2b^2}{3c^2} - 2\frac{b^2}{c^2}\cosh^{-1}\frac{b+c}{b}\right] \tag{48}$$

and the aspect ratio is

$$A = \frac{2b+c}{c} \tag{49}$$

Drag.- The drag of the wing is expressed by equation (31b). The drag of the cone alone is,

$$C_{D_c} = \frac{\pi\delta^4 c^2}{2(2bc + c^2)}\left(2\cosh^{-1}\frac{1}{\delta} - 1 + \delta^2\right) \tag{50}$$

However, a drag also arises because the wing induces a pressure field around the cone. In a first approximation, this drag may be taken as the frontal area of the half-cone times the pressure induced by the wing along its center line, that is, from equation (20) at $y = z = 0$.

$$C_{D_{h-c}} = \frac{2\alpha\delta^2 c}{2b + c} \tag{51}$$

If α is taken as some product of δ, the optimum ratio of the wing angle of attack to the cone half-angle is found by equation (29) and the optimum drag factor from equation (28).

DISCUSSION OF RESULTS

A sketch of each of the models analyzed in the previous sections is shown in figure 1. The lift and drag coefficients and the parameter σ as predicted by linear theory for the models without fuselages are shown in figures 2 and 3. The values predicted for the models with fuselages are shown in figures 4 through 7. These results may be used by a designer interested in an aircraft utilizing interference effects between surfaces resembling those studied herein.

The purpose in considering the models shown in figure 1 is to study the effect of the shape, location, and deflection of the various surfaces on the lifting efficiency of the airfoil system.[5] The question is whether indirect lift devices are worth considering.

The lifting characteristics of the systems shown in figure 1 can best be compared by considering the drag factor $C_{D_i}/\beta C_L^2$ (see eq. (2)) as discussed earlier. The drag factor for the models analyzed is shown in figures 8, 9, 10, and 11 as a function of reduced aspect ratio βA. The curve for the triangular wing is shown in the figures as a reference curve. It is well known that when the flow velocity perpendicular to the leading edge is supersonic, $\beta A > 4$, the lift-curve slope is $4/\beta$ and the drag factor is 0.25. Also shown as a reference curve is the theoretical minimum value of the drag factor for slender planar wings. This minimum or optimum curve serves to indicate whether the airfoil system being considered is more efficient than is theoretically possible with a planar system.

[5]The effect on performance when the airplane is flying at an off-design Mach number is not considered.

It is immediately obvious from figures 8(a) and 9(a) that, when the drag factor is based on the plan form plus fin area, the models are not nearly so efficient as a good planar wing. The figures 8(a) and 9(a) apply to the physical cases wherein the fins are added to the aircraft. The more promising situation is when the coefficients are based on the plan-form area (figs. 8(b) and 9(b)), that is, when the vertical surfaces are assumed to be usable for other purposes, such as lateral control. The remainder of the discussion will be restricted to the cases when the coefficients are calculated using the plan-form area as the reference area. In other words, it is assumed that the vertical surfaces are a necessary part of the aircraft for reasons other than lift augmentation.

The curves of the drag factor (figs. 8(b) and 9(b)) for the models when all the surfaces are deflected in the optimum ratio (solid curves) are noted to be the lowest of the results calculated. At low values of reduced aspect ratio these models are superior to the optimum planar wing expressed by the theoretical minimum curve. These results point out two important conclusions: (1) The lifting efficiency of aircraft can in certain cases be improved over planar systems by indirect lift devices. (2) The largest improvement is achieved if all of the available surfaces of the airfoil system are deflected in the correct ratio (see, e.g., eqs. (28) and (29)).

Various modificiations were made to the simple airfoil system, Model 1, and each represents an improvement in the lifting efficiency or a reduction in the drag factor as shown in figure 10. The addition of fins (undeflected) to the reverse swept wing results in a notable improvement in the lifting efficiency. A further gain is achieved by deflecting the fins and wing properly, and by increasing the lift by removing that portion of the wing which is carrying a negative indirect lift force from the fin, as discussed in the analysis of Models 2 and 7. This illustrates the importance of making certain that the entire surface of the airfoil system works positively. Another reduction in the drag factor tells one to contour the fuselage, even at the expense of losing the overlap lift in the center of the wing, Models 6 and 7. All of the surfaces of Model 7 have been cut and deflected to produce the best configuration shown in this figure.

The essential requirements of the wing of the airfoil systems studied are that it lie in the region of influence of the fin and that it serve as a barrier between the opposite pressure fields induced by the upper and lower fins. These considerations and the fact that the airfoil systems must be reasonably simple to analyze restrict the wing plan form somewhat. Therefore, with three exceptions, the wings studied in this report are of constant chord with leading and trailing edges swept along the Mach lines. It is to be noted in figure 8, that the drag factor of this sonic leading-edge wing is not near the theoretical minimum for planar wings. The problem treated is one of taking a wing which is not too efficient and trying to make it better than something which is already good. An alternative

problem is to take a good wing and try to improve it by addition of body contouring and/or fins. This is attempted in the design of Model 9, but the choice of the wing and body contour is not good. In order to facilitate the analysis of the model the body contour had to be taken small enough so that the pressures induced by it did not bleed over the leading edge. Since the taper ratio of this wing is 1/4, only 2/5 of the wing surface felt the influence of the body contour. As a result, the wing alone and the combination are about equally efficient. Both results fall on one single curve shown in figure 9. The conclusion drawn from this is that when a device which is not too efficient is added to one which is efficient, the optimum for the combination is only slightly better than the efficient part by itself. The largest improvement is realized when the fin and wing are about equally efficient. A combination using a good wing approaching the theoretical minimum which could also utilize indirect lift to a great extent is the desired combination.

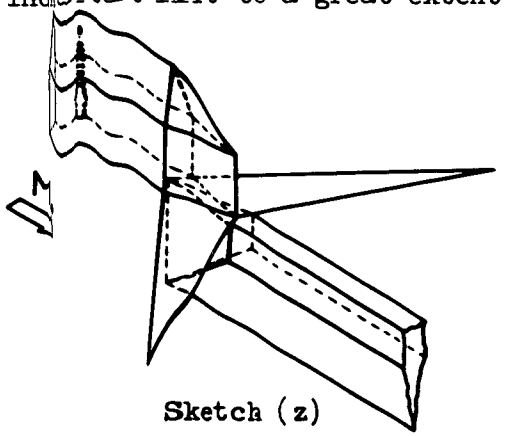

Sketch (z)

One such airfoil system which can be analyzed theoretically is shown in sketch (z). The model consists of an arrowhead wing with subsonic leading edges and sonic trailing edges with the indirect lift induced by flat vertical sections on the fuselage sides which are just high enough so that their upper and lower ends do not influence the wing. The extreme height of these flat sections enables one to find the pressures on the wing quite simply from linearized conical flow theory[6]

[6]The conical flow solution (provided by Doris Cohen of the Ames Aeronautical Laboratory staff) for the axial velocity induced on the wing by the fuselage wedge is

$$\frac{u}{U} = \frac{2\delta}{\pi} \operatorname{Re}\left[\tan^{-1}\sqrt{\frac{m^2-(y/x)^2}{1-m^2}} + \frac{m^2\sqrt{1-m^2}}{\sqrt{m^2-(y/x)^2}}\frac{K}{E}\right]$$

where K and E are complete elliptic integrals of the first and second kind with modulus $\sqrt{1-m^2}$. The lift and drag are then found as

$$C_{L_{v-h}} = \frac{4\delta(1-m)}{\pi m}\left\{\frac{m}{\sqrt{1-m^2}} + \frac{2m^2-1}{1-m^2}\sin^{-1}m + \frac{\pi m^2}{2(1-m^2)} + \frac{2K}{\sqrt{1-m^2}\,E}\left[m^3 + \frac{m^2}{\sqrt{1-m^2}}\sin^{-1}m + \frac{\pi m^2}{2(\sqrt{1-m^2})}\right]\right\}$$

$$C_{D_t} = \frac{\pi m\sqrt{1-m^2}}{1-m}\left[\frac{\delta^2}{E^2}\left(\sigma + \frac{2}{\pi}\sqrt{1-m^2}K\right)^2\right]$$

$$C_{D_{v-v}}\Big|_{\frac{y}{x}\geq 0-\epsilon} = \frac{8\delta^2(\sqrt{1-m^2}-1+m)}{m} + \frac{2\delta^2}{\pi m}\sqrt{\frac{1-m}{1+m}}\left(\frac{m^2K^2}{E} + \frac{\pi\sqrt{1-m^2}}{2} - E\right)$$

$$C_{D_{h-v}}\Big|_{\frac{y}{x}\leq 2\geq 0-\epsilon} = \frac{4\delta\alpha m}{1+m}\left(\frac{K}{E} - 1\right)$$

The expressions for $C_{D_{v-v}}$ and $C_{D_{h-v}}$ become more complicated for reduced aspect ratios below 6 ($m = 0.6$).

but makes the proportions of the model impractical. The drag factor for the model when the wing is undeflected ($\alpha = 0$) and the wedge is present ($\delta \neq 0$) and when the wing is deflected ($\alpha \neq 0$) in combination with the wedge ($\delta \neq 0$) is shown in sketch (aa). The results for the arrowhead wing can be found from reference 8. A sizable improvement over the arrowhead wing is achieved by deflecting the fuselage sides in combination with the wing. However, thus far, the analysis can be carried out only for rather high fuselages and a model of comparable efficiency which is of more practical proportions is yet to be desired.

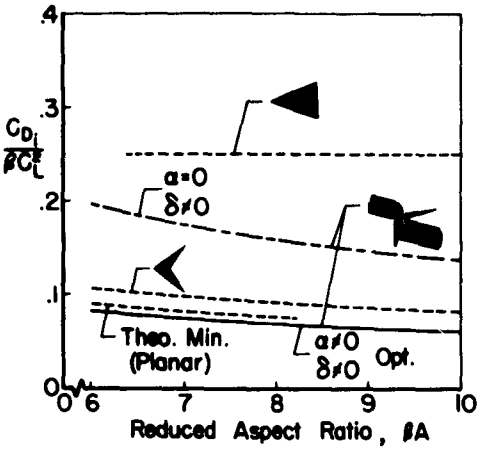

Sketch (aa)

The several different fin configurations which were studied permit a limited discussion of the effect of fin shape on the lifting efficiency. It is seen from figure 8(b) that the airfoil combinations with unswept leading-edge fins, Models 1 and 2, are more efficient than when the leading edge is swept along the Mach line as with Model 3. This is true for all values of reduced aspect ratios for the curved-trailing-edge wing plan form, Model 2, but only for the lower values for the constant-chord wing, number 1. It is interesting to note that although the drag of the fin shapes for Models 1 and 3 are the same, the pressure shadow on the wing is very different.

For wings of reduced aspect ratio above 10, it may be advantageous to go to taller fin shapes such as those of Model 4. The rectangular section of the fin increases the region on the wing where the pressure distribution is of the two-dimensional type. The extent of this region increases roughly as the square of the fin height (see eq. (23)), resulting in an efficient model at large aspect ratios. The drag factor for Model 4 is not presented since the values are off scale for values of reduced aspect ratio below about 8.

If the fins were to lean outward a slight amount, they would not only generate indirect lift on the wing, but carry a component themselves. A simple problem to investigate is the limiting case shown in sketch (m) as Model 5. This case is the same as twisting the wing and does not permit use of vertical surfaces already on the airplane. The results of Model 5 may be applied to wing-tip control surfaces.

The vertical surfaces on the aircraft might be modified to receive a push from the pressure field induced by the wing or another vertical surface. This is illustrated by the wing-body combinations 6 and 7 where the fuselage is contoured to receive a thrust from the fin and wing pressure fields. Typical values of the interference of the fin on the

body are shown in figure 5 and the resulting thrust is shown in figure 6. This principle could be applied to other types of fins and wings which appear more structurally feasible.

Model 8, sketch (v), is designed with the thought that it would be applicable to conventional aircraft as shown in sketch (q). The fuselage is contoured to generate indirect lift on the wing and the fins serve as end plates. The control of the airplane is achieved by simply moving the fins in the proper combination to produce turning, rolling, or pitching motions. Roll and pitch control is also obtained by deflection of the fuselage sides. The parameters calculated for fin deflection only may be used in the design of this type control system. An advantage worth noting is that the lift can be changed without first pitching the airplane or missile.

The drag factor for the indirect lift from the half-cone is shown for several cone angles in figure 11. (The lower solid curve is the drag factor for $\delta = 15^{\circ}$ and the wing deflected the correct amount.) It may be reasoned that the half-cone body is the entire fuselage rather than a perturbation body. The pressure drag of the half-cone would then appear in equation (2) as part of C_{D_o} instead of part of C_{D_i}. The dotted line in figure 11 is the drag factor for Model 10 when the half-cone body is taken as the entire fuselage. A comparison of the results in figure 11 with those in figures 8 and 9 shows that the efficiency of the half-cone model is not so good as some of the other airfoil systems analyzed. This can be attributed to the fact that the pressure shadow induced by a body of revolution is not so intense as that from a flat surface; and, the wing used is not so efficient as the one used on the other models.

It might also be asked whether the gain from the end plates at supersonic speeds is greater than at subsonic speeds. The results in reference 2 show that at subsonic speeds the lift is increased enough to offset the added frictional drag of the fins. However, it is also pointed out that approximately the same gain could be realized by laying the end plates horizontally as extensions to the wing span. At supersonic speeds the percentage gain realized when the end plates are used as extensions to the wing span is not so high as that possible when the same area is used as end plates.

The models discussed were analyzed by linear theory in which it is assumed that the direction of the Mach waves throughout the disturbed flow field is the same as in the free stream. The plan-form geometry was designed around this assumption which, to a first order for thin wings at small angles of attack, is permissible. However, in these special designs the location of particular surfaces must be such that they can benefit from the influence of another surface. The boundaries of these influence regions or pressure fields lie along shock or Mach waves from the deflected surfaces. Hence, if the local wave angles differ greatly

from the free-stream angles and the shape or location of the surfaces is not adjusted accordingly, a part of the desired gain may be lost. Similar considerations apply to flight at an off-design Mach number.

Two examples are shown in figures 12 and 13 so that the comparison can be made between the wave pattern calculated by linear theory and the more exact wave patterns computed by the shock-expansion method. The model shown in figure 12 is similar to Model 4. It is to be noted that the compression regions lie ahead of and the expansion fan behind the linearized locations. Also note that the upper and lower edges in the more exact theory do not match.

A bottom view of the linearized and the more exact wave pattern for a 10° half-cone mounted on the bottom of a swept wing is shown in figure 13. The more exact wave pattern was found by the method of characteristics. The line in the pressure field along which the lifting pressures go to zero is indicated as the $C_p = 0$ line. It is to be noted that the linear wing plan form lies within the lifting pressure field.

CONCLUDING REMARKS

It is hoped that the foregoing analysis will provide some interesting and instructive examples of the type of interference effects that may be utilized at supersonic speeds. While no far-reaching conclusions should be drawn from the examples given, it is clear that in some cases the lift-drag ratio can be improved noticeably if interference effects between existing vertical surfaces and the wing are used advantageously. Several of the models studied are more efficient at low aspect ratios than is theoretically possible with planar wings. A configuration of comparable efficiency with a very high narrow fuselage is found for the higher values of reduced aspect ratio. The efficiency of the whole airplane can, in certain cases, be improved by indirect lift devices which can also be used for control purposes.

Ames Aeronautical Laboratory
National Advisory Committee for Aeronautics
Moffett Field, Calif., Dec. 8, 1955

REFERENCES

1. Reid, Elliott G.: The Effects of Shielding the Tips of Airfoils. NACA Rep. 201, 1925.

2. Hemke, Paul E.: Drag of Wings with End Plates. NACA Rep. 267, 1927.

3. Scholkemeier, F. W.: Flugel mit Endscheiben. Ministry of Supply, Völkenrode Monograph, Reps. and Trans. 541, 1948. (Also published as Ministry of Supply, Völkenrode Monograph GDC/2472)

4. Gorgui, M. A.: The Effect of Delta Vanes on Supersonic Wings. The Aeronautical Quarterly, vol. V, pt. 4, Nov. 1954, pp. 251-279.

5. Clements, Harry R.: Canted Adjustable End Plates for the Control of Drag. Aeronautical Engineering Review, vol. 14, no. 7, July 1955, pp. 40-44.

6. Ferri, Antonio, Clarke, Joseph H., and Casaccio, Anthony: Drag Reduction in Lifting Systems by Advantageous Use of Interference. PIBAL Rep. 272, Polytechnic Institute of Brooklyn, Dept. of Aeronautical Engineering and Applied Mechanics, May 1955.

7. Lagerstrom, P. A.: Linearized Supersonic Theory of Conical Wings. NACA TN 1685, 1950.

8. Jones, R. T., and Cohen, Doris: Aerodynamics of Wings at High Speeds. (Sec. A of Aerodynamic Components of Aircraft at High Speeds. vol. VII of High Speed Aerodynamics and Jet Propulsion, A. F. Donovan and H. R. Lawrence, ed., Princeton Univ. Press, In Press.)

9. Cohen, Doris, and Friedman, Morris D.: Theoretical Investigation of the Supersonic Lift and Drag of Thin, Sweptback Wings With Increased Sweep Near the Root. NACA TN 2959, 1953.

10. Harmon, Sidney M., and Jeffreys, Isabella: Theoretical Lift and Damping in Roll of Thin Wings with Arbitrary Sweep and Taper at Supersonic Speeds. - Supersonic Leading and Trailing Edges. NACA TN 2114, 1950.

11. Cohen, Doris: Formulas for the Supersonic Loading, Lift, and Drag of Flat Swept-back Wings with Leading Edges Behind the Mach Lines. NACA Rep. 1050, 1951.

12. Hayes, Wallace D.: Reversed Flow Theorems in Supersonic Aerodynamics. North American Aviation Inc. Rep. No. AL-755, Aug. 20, 1948.

13. Heaslet, Max. A., and Spreiter, John R.: Reciprocity Relations in Aerodynamics. NACA Rep. 1119, 1953.

14. Malvestuto, Frank S., Jr., Margolis, Kenneth, and Ribner, Herbert S.: Theoretical Lift and Damping in Roll at Supersonic Speeds of Thin Sweptback Tapered Wings with Streamwise Tips, Subsonic Leading Edges, and Supersonic Trailing Edges. NACA Rep. 970, 1950.

15. Heaslet, Max. A., and Lomax, Harvard: Supersonic and Transonic Small Perturbation Theory. Sec. D of General Theory of High Speed Aerodynamics, W. R. Sears, ed., pp. 122-344. Vol. VI of High Speed Aerodynamics and Jet Propulsion. Princeton Univ. Press, 1954.

16. Byrd, Paul F., and Friedman, Morris D.: Handbook of Elliptic Integrals for Engineers and Physicists. Vol. LXVII of Grundlehren der Mathematischen Wissenschaften in Einzeldarstellungen. Berlin, Springer-Verlag, 1954.

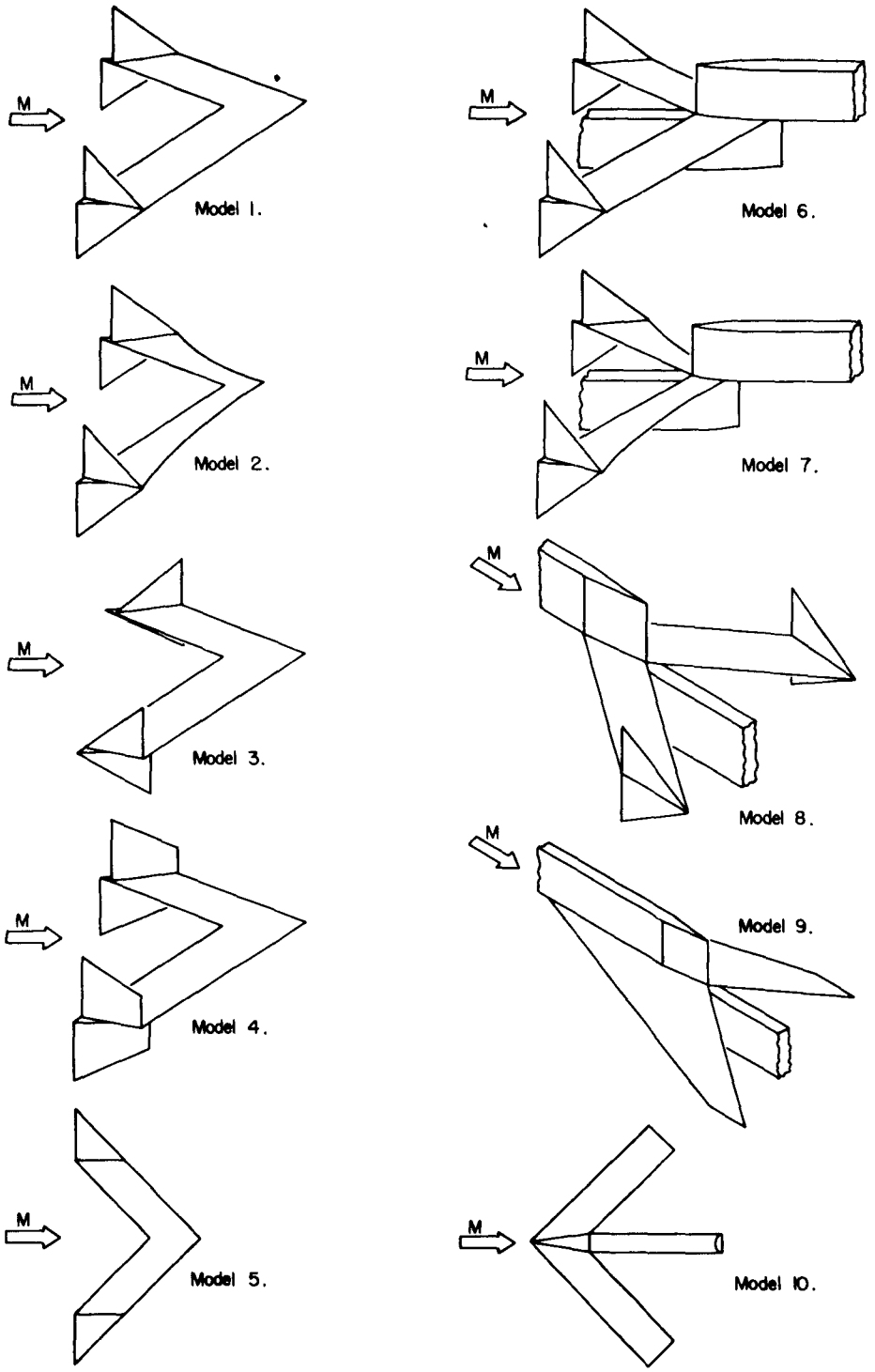

Figure 1.- Sketch of the models analyzed.

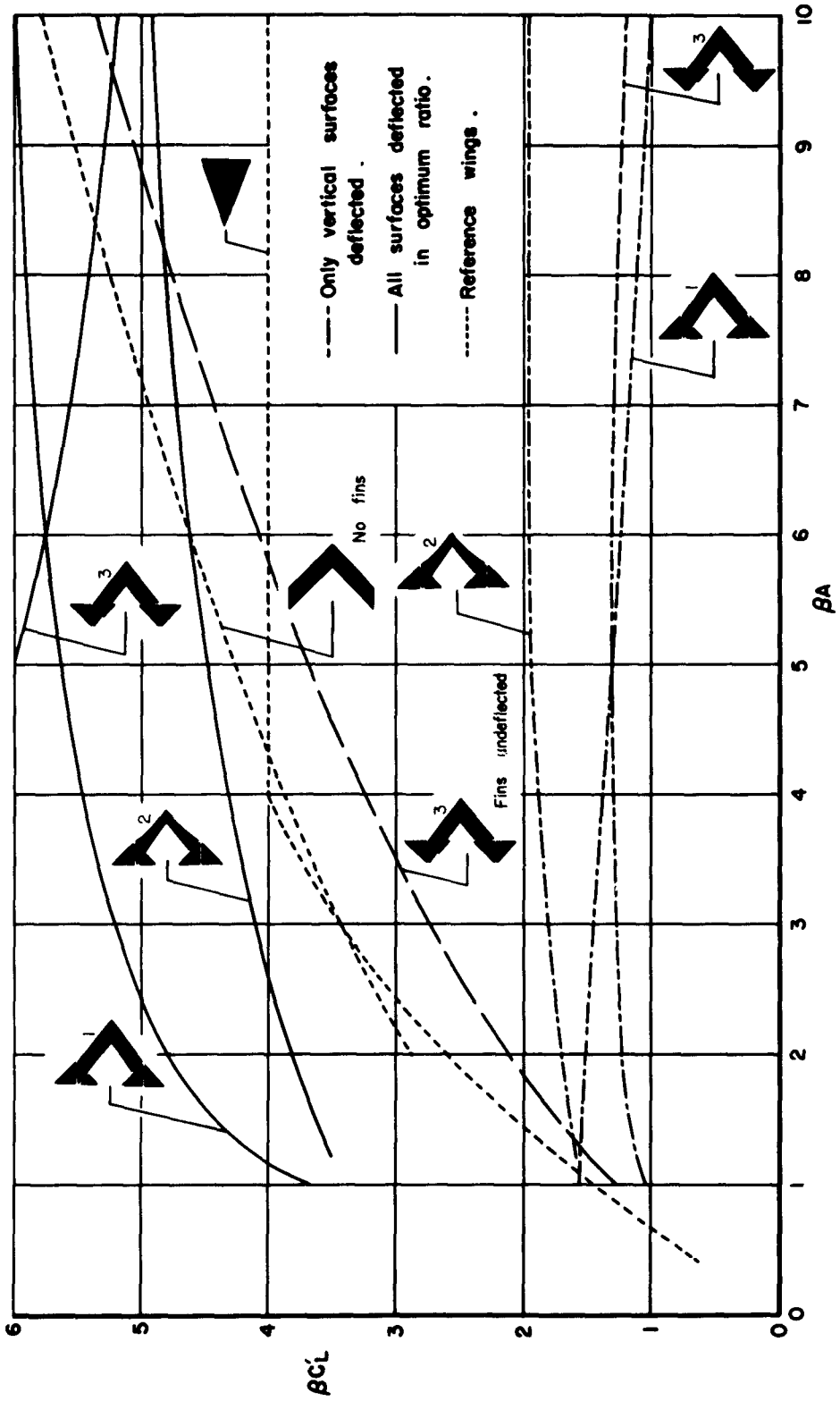

(a) Lift.

Figure 2.- Force coefficients for several arrangements of wings with vertical fins; coefficients based on plan-form area plus fin area.

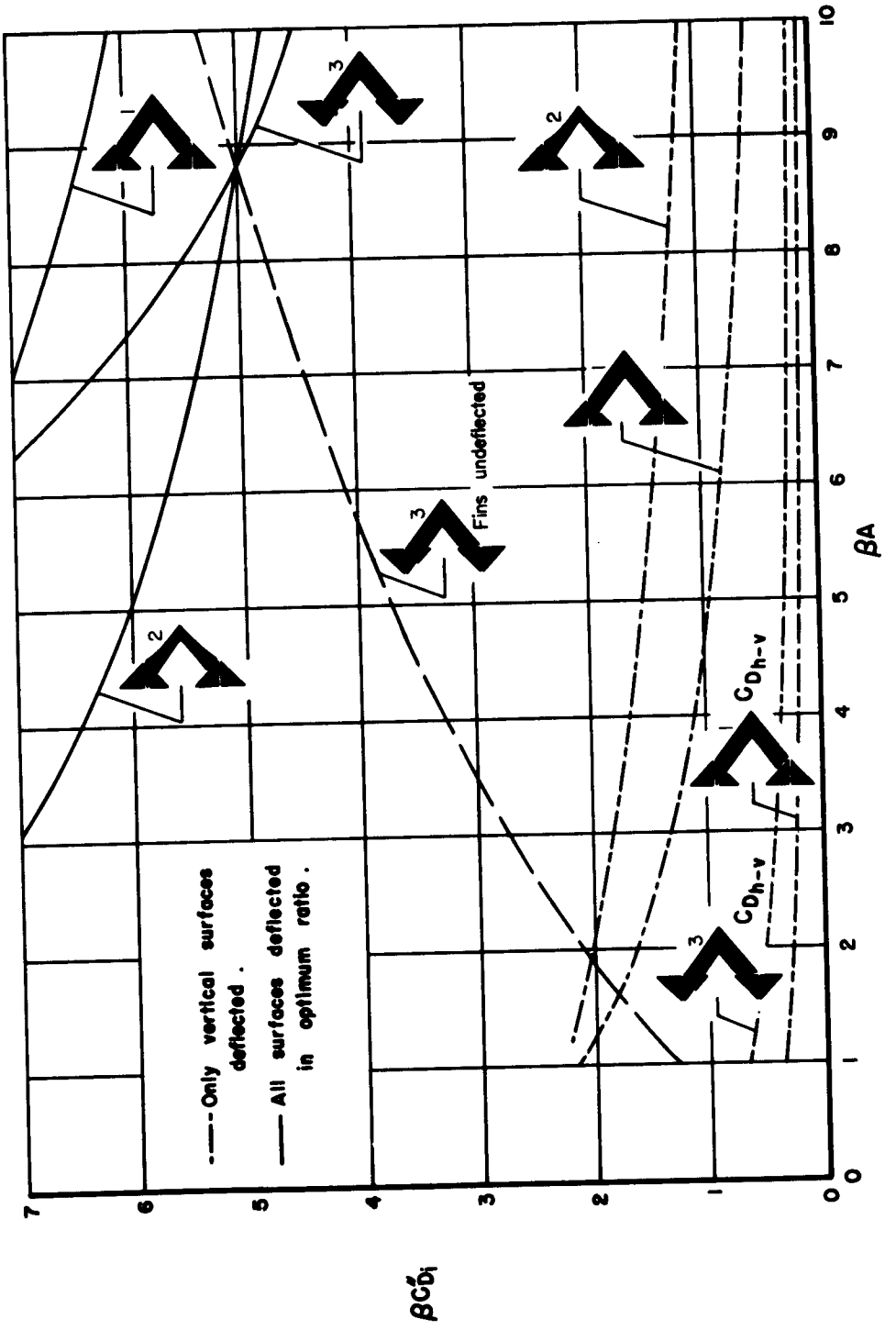

(b) Drag.

Figure 2.- Concluded.

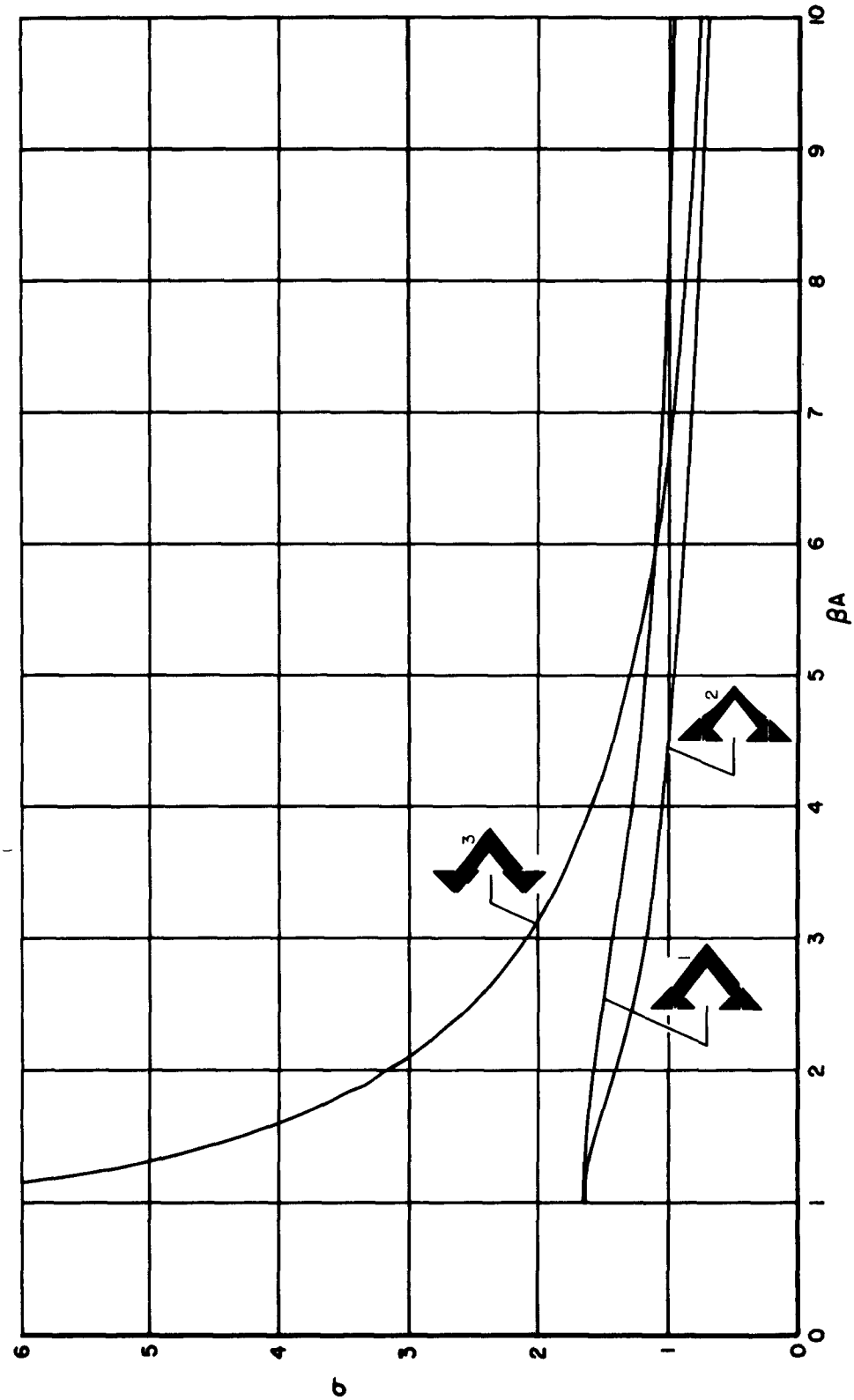

Figure 3.- Optimum ratio of angle of attack of horizontal to vertical surface.

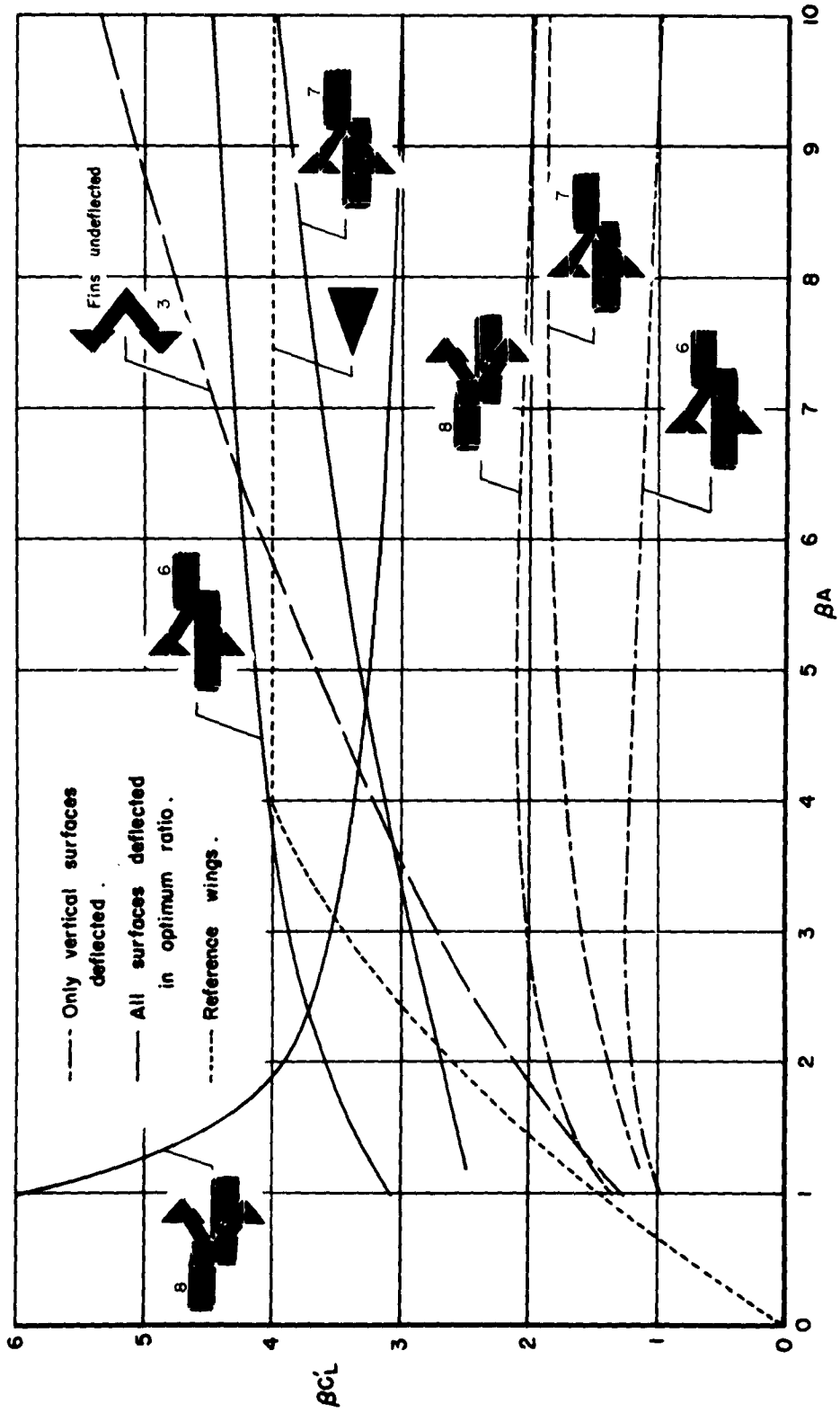

(a) Lift.

Figure 4.- Force coefficients for several models with fuselages; coefficients based on plan-form area plus fin area.

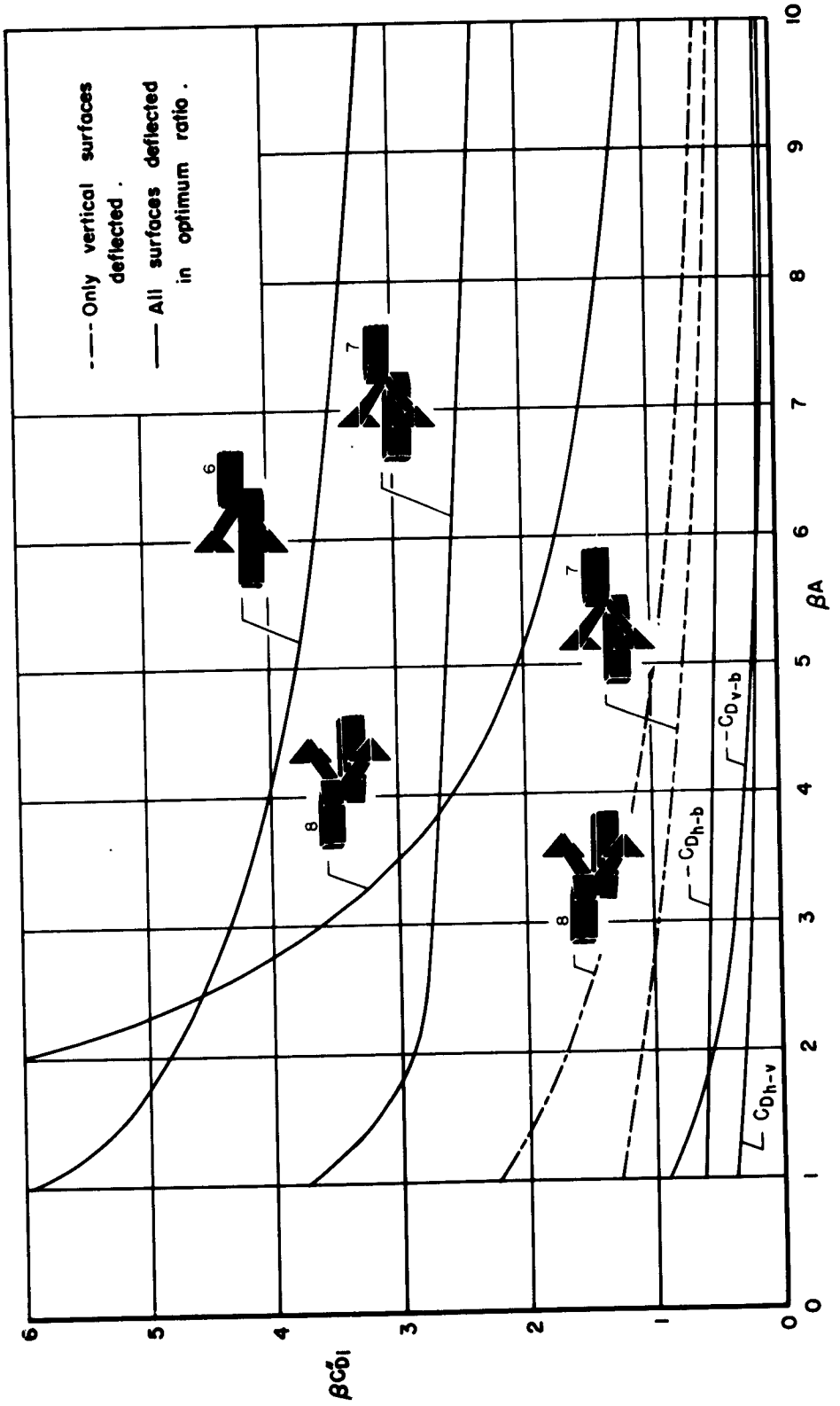

(b) Drag.

Figure 4.- Concluded.

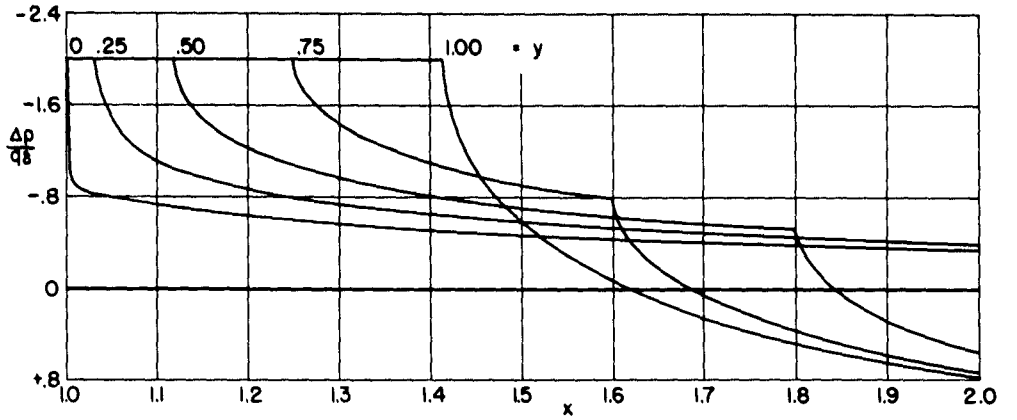

(a) Pressure

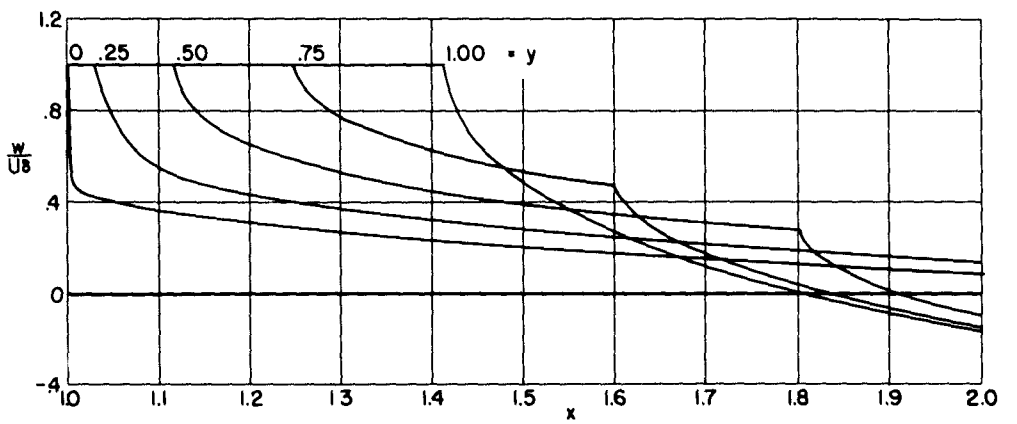

(b) Slope

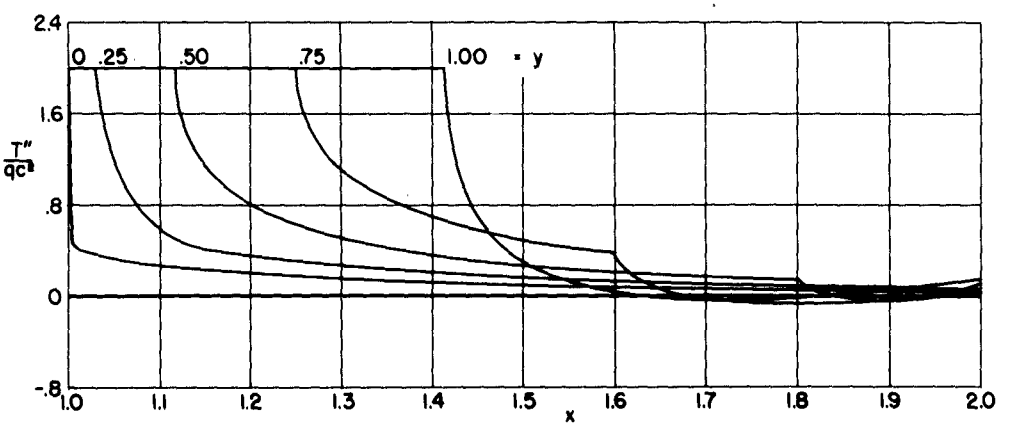

(c) Thrust

Figure 5.- Typical values of local quantities used in finding thrust on the fuselage of Models 6 and 7; b/c = 1.0.

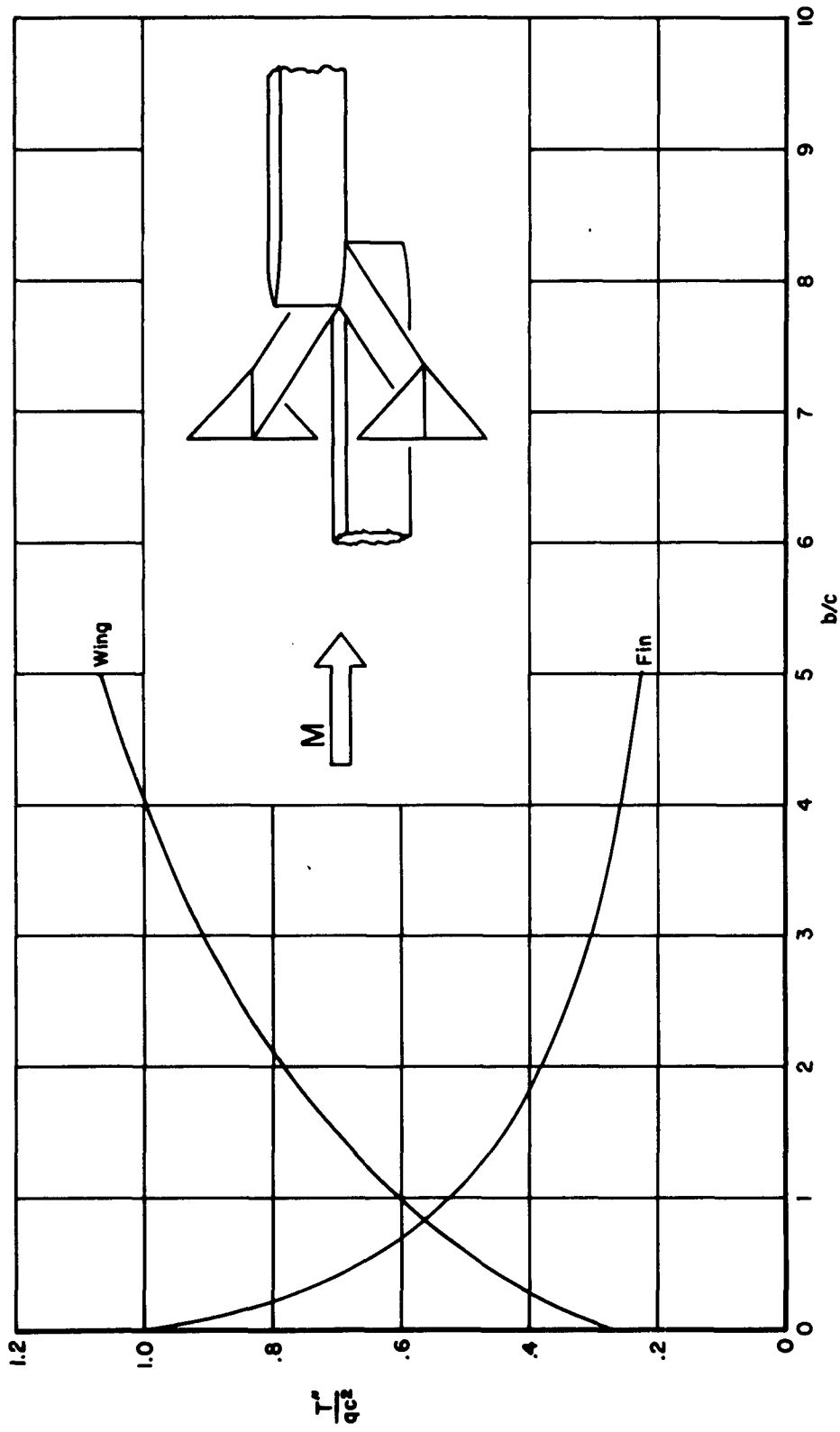

Figure 6.- Thrust induced on a properly contoured fuselage by fin and wing as a function of wing span.

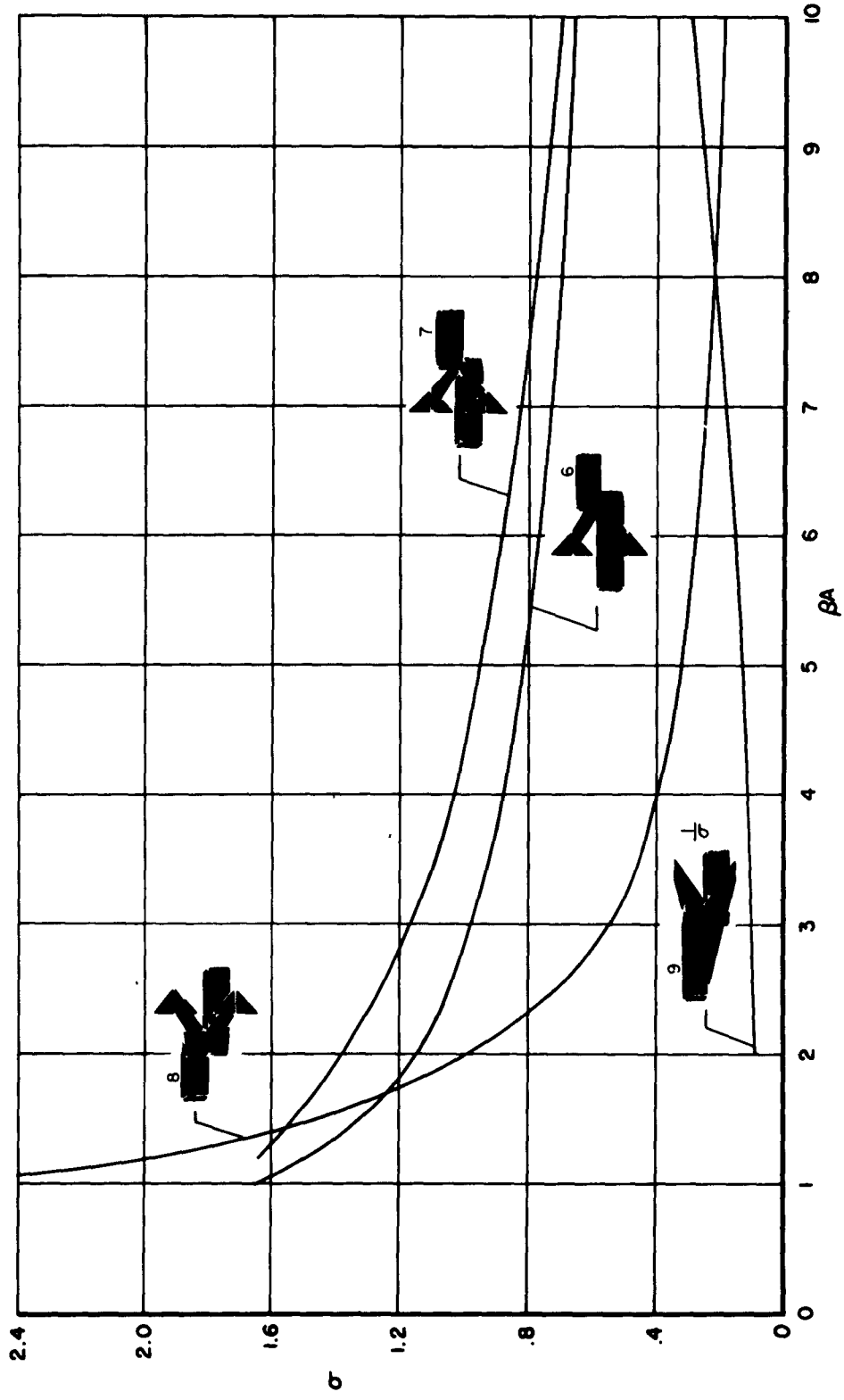

Figure 7.- Optimum ratio of angle of attack of horizontal to vertical surface for several models with fuselages.

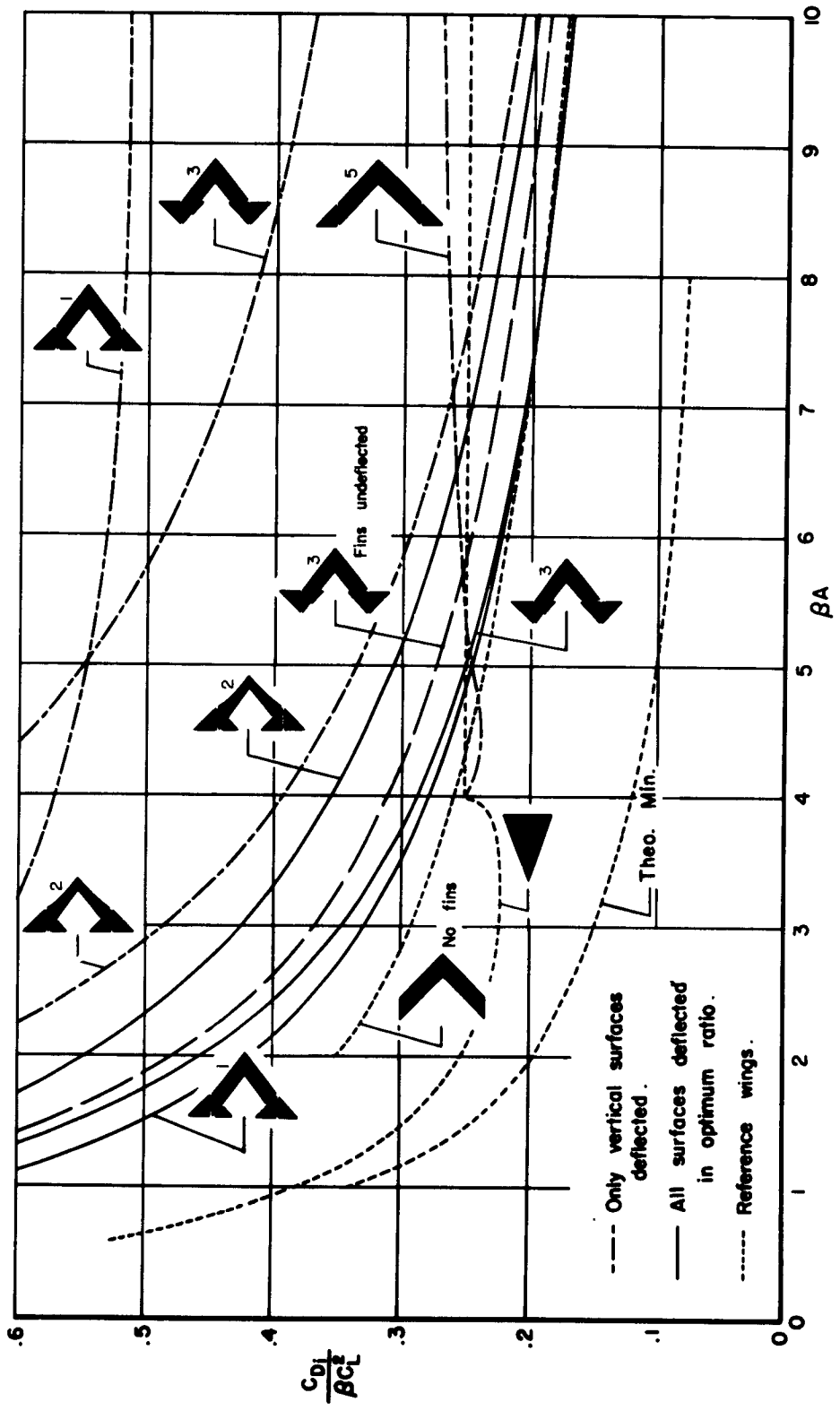

(a) Coefficients based on plan-form plus fin area.

Figure 8.- Drag factor for several airfoil combinations without fuselages.

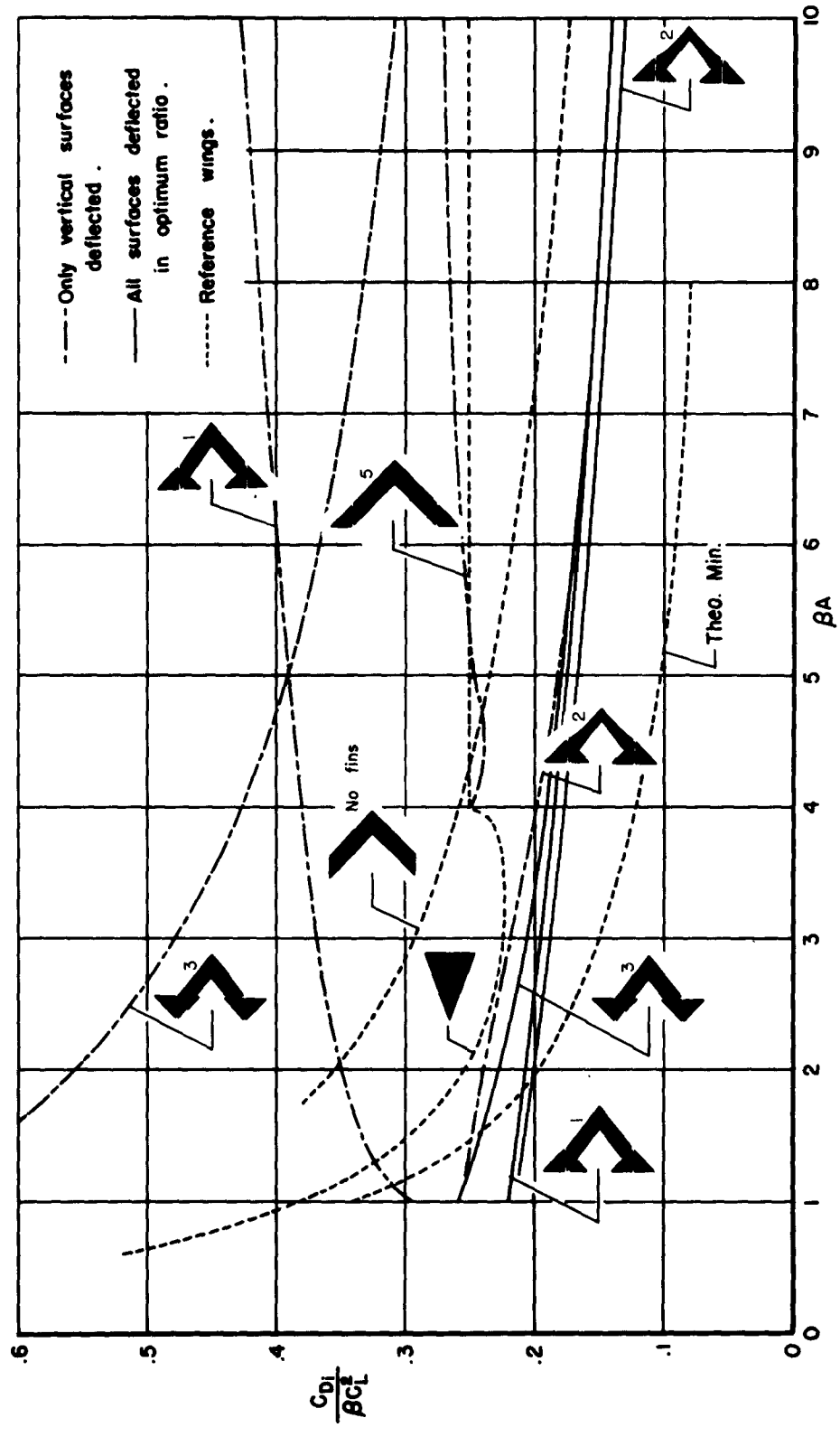

(b) Coefficients based on plan-form area.

Figure 8.- Concluded.

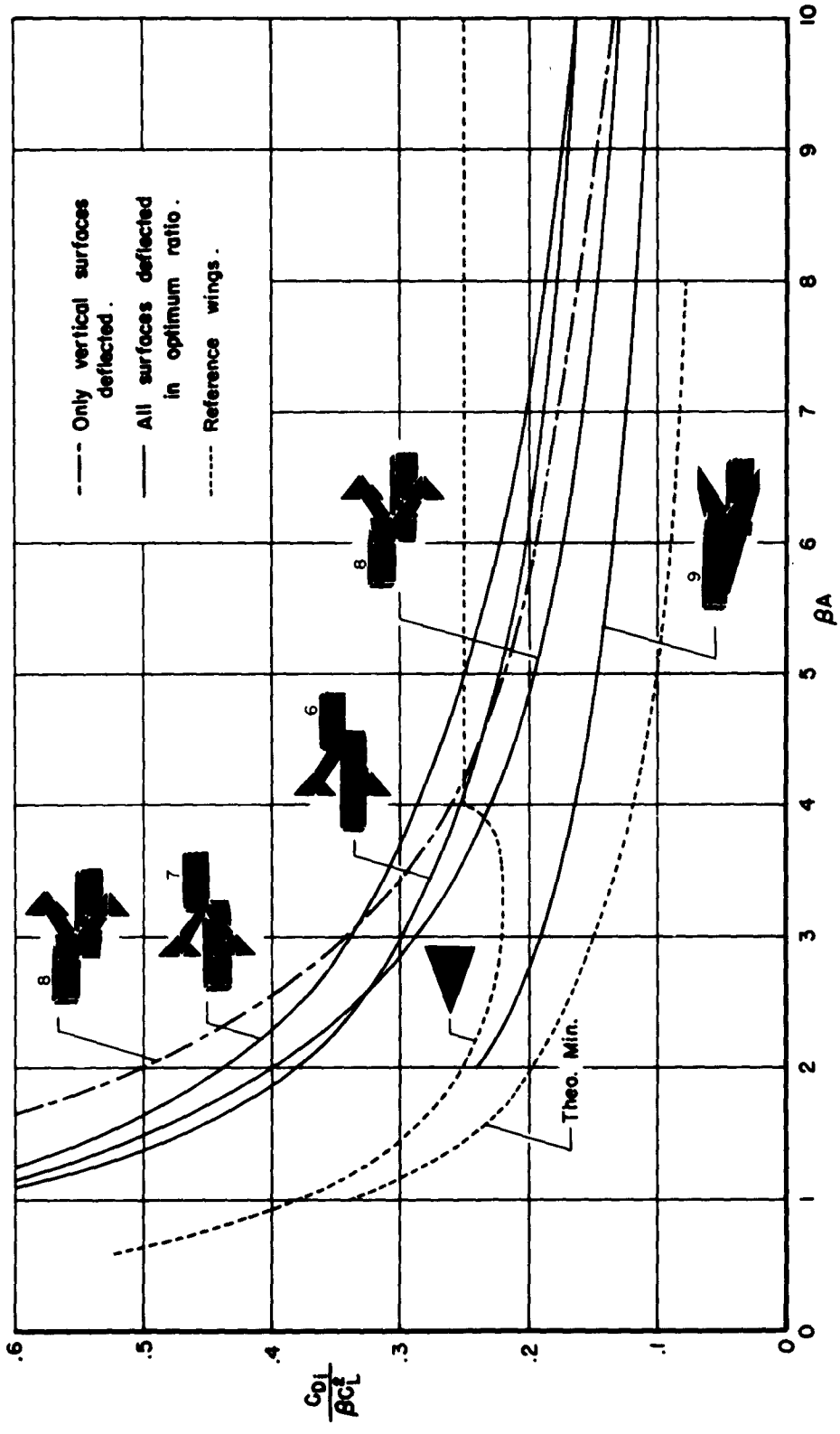

(a) Coefficients based on plan-form plus fin area.

Figure 9.- Drag factor as a function of aspect ratio for several models with fuselages.

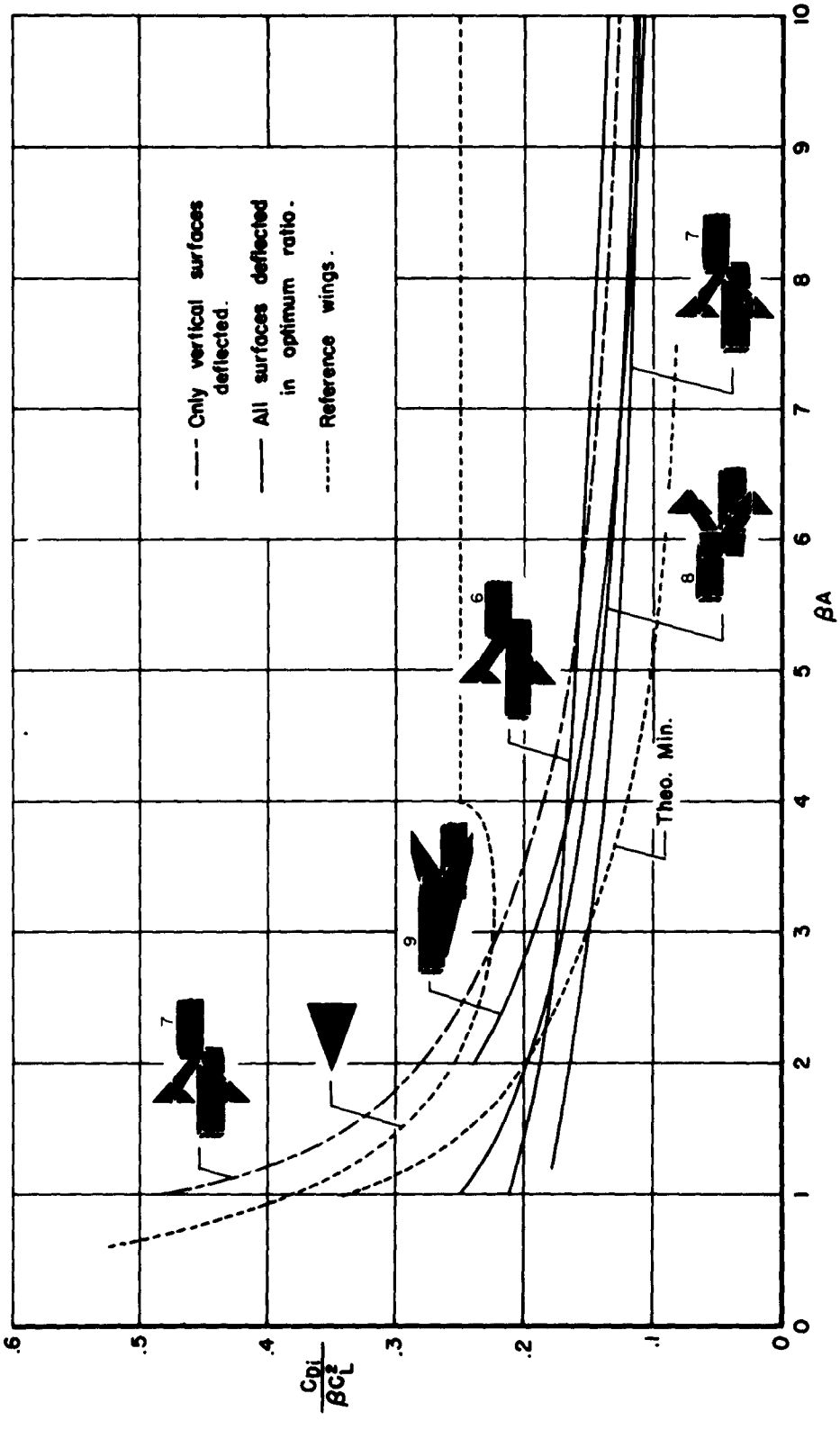

(b) Coefficients based on plan-form area.

Figure 9.- Concluded.

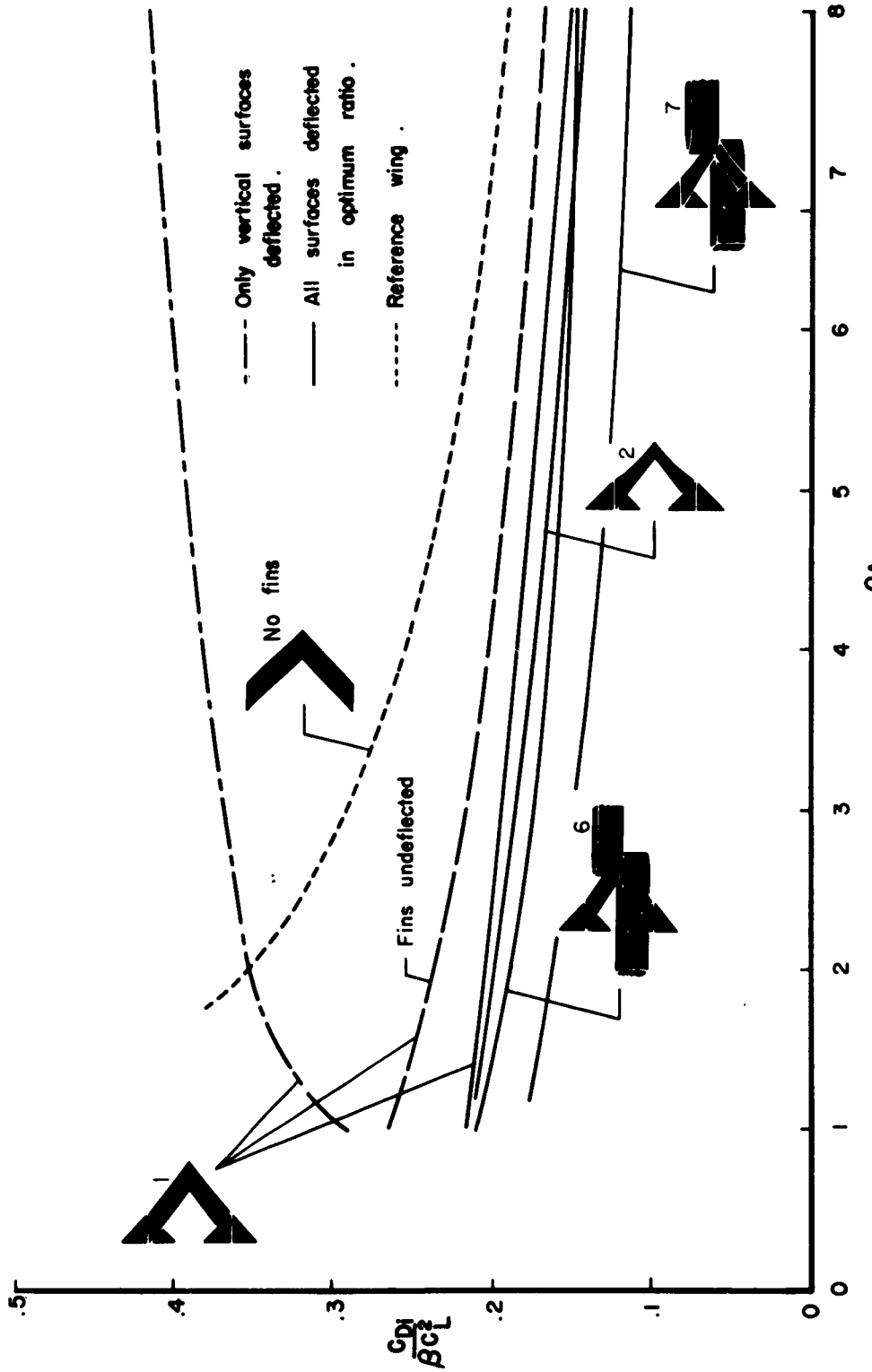

Figure 10.- Drag factor for airfoil systems with triangular end plates whose leading edges are unswept. Reference area for the coefficients is the plan-form area.

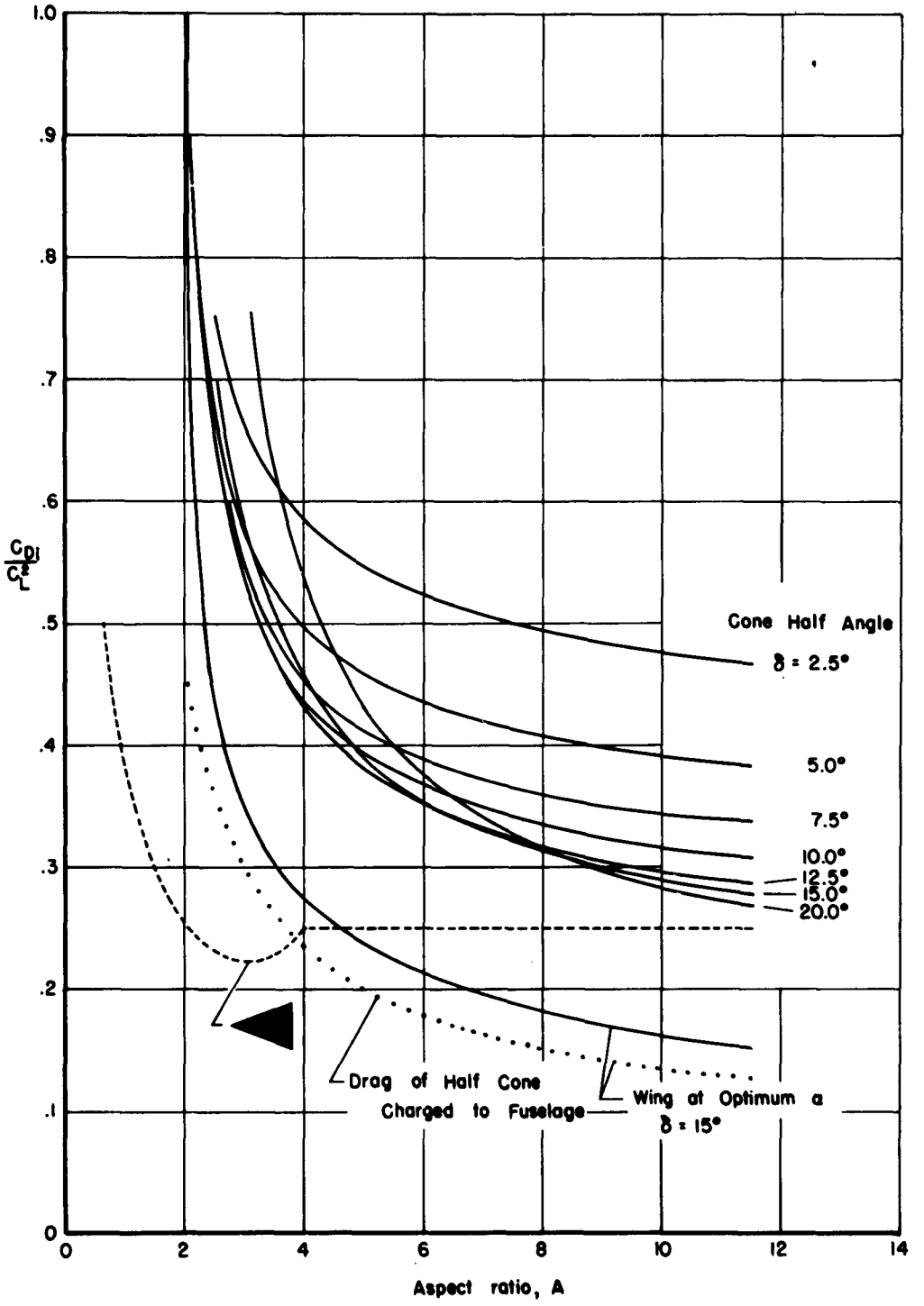

Figure 11.- Drag factor for a half cone mounted under a swept wing at a Mach number of $\sqrt{2}$.

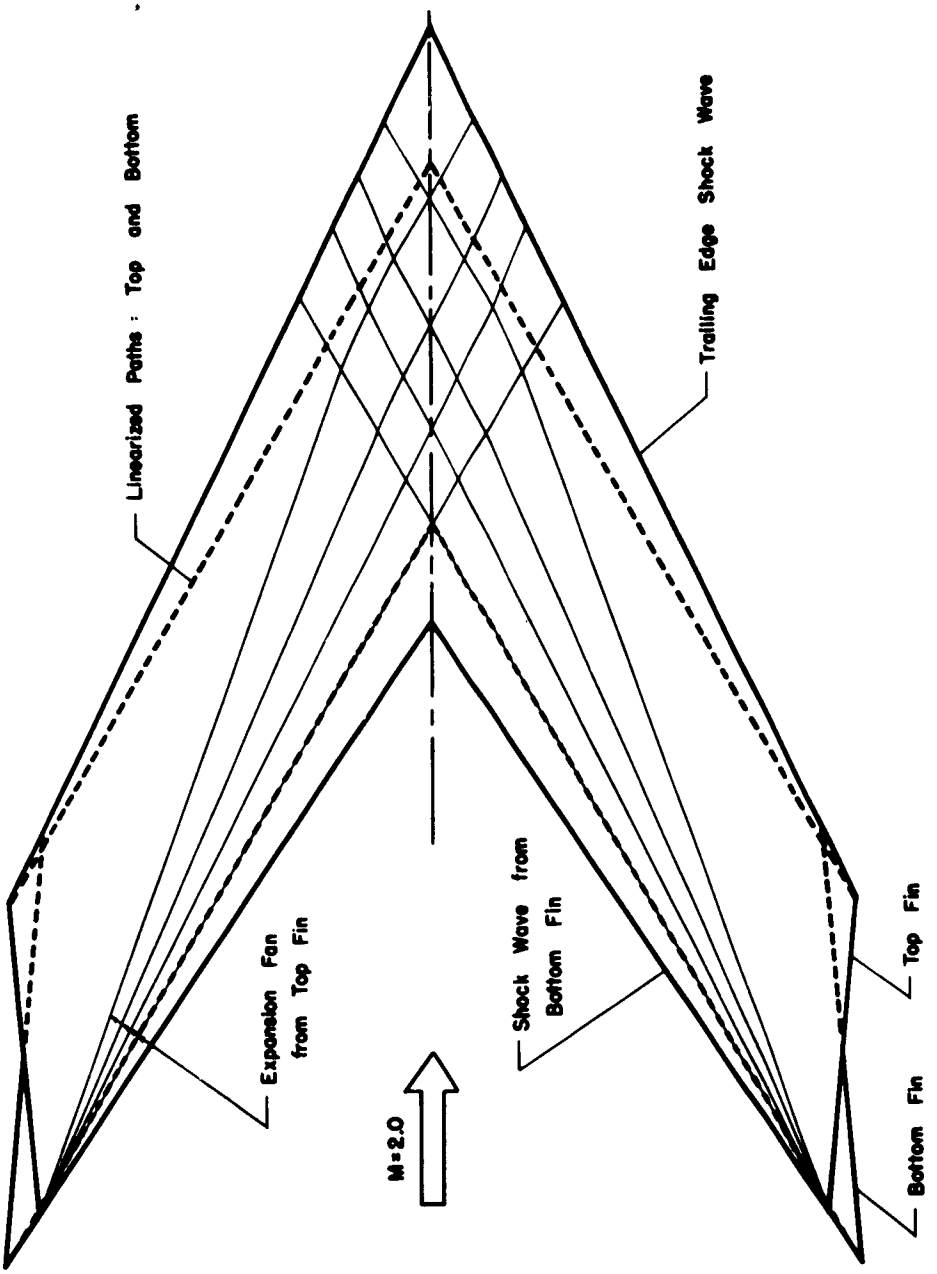

Figure 12.- Sketch showing the linearized and more exact locations of the paths of the Mach lines and shock waves on a finned wing flying at M = 2 and $\delta = 5^{\circ}$.

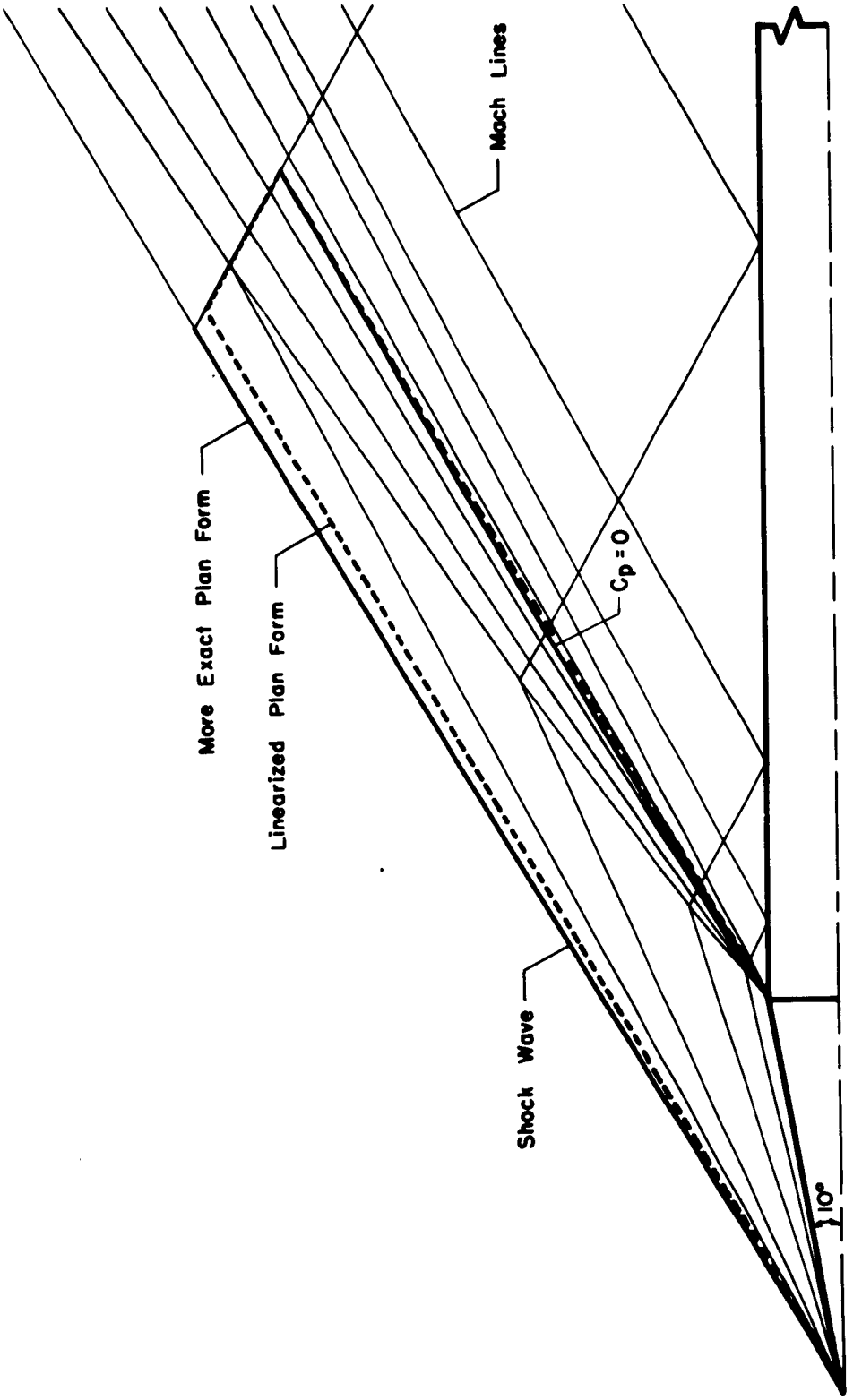

Figure 13.- Plan view of linearized and true wave patterns for a half cone mounted under a swept wing; $M_\infty = 2.0$.

NACA - Langley Field, Va.